[American Journal of Science, Vol. 314, January, 2014, P. 1–42, DOI 10.2475/01.2014.01]

American Journal of Science

MESOZOIC INTRAPLATE GRANITIC MAGMATISM IN THE ALTAI ACCRETIONARY OROGEN, NW CHINA: IMPLICATIONS FOR THE OROGENIC ARCHITECTURE AND CRUSTAL GROWTH

TAO WANG*,**,†, BOR-MING JAHN***, VICTOR P. KOVACH§, YING TONG*, SIMON A. WILDE§§, DA-WEI HONG*, SHAN LI*, and EKATERINA B. SALNIKOVA§

ABSTRACT. **The Central Asian Orogenic Belt (CAOB) is the world's largest Phanerozoic accretionary orogen and is the most important site for juvenile crustal growth in the Phanerozoic. In this work, we employed U-Pb zircon geochronology to identify the early and middle Mesozoic intraplate granitic intrusive events in the Chinese Altai segment of the southern CAOB in order to better understand the crustal architecture of the CAOB. We also used whole-rock geochemical, Sr-Nd isotopic and zircon Hf isotopic data to constrain the generation for these granitic rocks and to evaluate the implications for vertical crustal growth in this region. The Early Mesozoic granitic intrusions were emplaced between 220 and 200 Ma in the central Altai "microcontinental terrane" (also widely referred to as Units 2 and 3). The granites have shoshonitic and high-K calc-alkaline affinities and show the characteristics of differentiated I-type granite. The whole-rock initial $^{87}Sr/^{86}Sr$ ratios (0.7058-0.7128) and $\varepsilon_{Nd}(210)$ values (−0.6 to −4.3), as well as the zircon $\varepsilon_{Hf}(t)$ values (−4.0 to +5.0) and two-stage Hf model ages (0.94-1.52 Ga), suggest that the granitic magmas were produced from a mixed source with both mantle-derived and recycled crustal components. The middle Mesozoic granites were emplaced at ~150 Ma in the southern Altai "accretionary terrane" (Units 4 and 5). They show A-type characteristics with the REE tetrad effect and have positive $\varepsilon_{Nd}(151)$ whole-rock values of +1.0 to +5.2 and two-stage Nd model ages (T_{DM2}) of 0.6 to 1.0 Ga. Zircon Hf data show positive zircon $\varepsilon_{Hf}(151)$ values of +1 to +8 and two-stage Hf model ages of 0.6 to 1.2 Ga. The Nd-Hf isotopic data suggest that the granitic magmas were derived from short-lived juvenile mantle-derived materials. Thus, the isotopic signatures of all the Mesozoic granites from the central (old terrane) and southern (young accretional terrane) Altai suggest that the basement of both terranes has retained its original nature. The data further imply that the Altai orogen has kept its original architecture of Paleozoic horizontal accretion during Mesozoic time, as commonly observed in accretionary orogens where horizontal tectonics are dominant. All the early Mesozoic intrusions in the Altai were emplaced in an intraplate anorogenic setting; hence are distinguished from the contemporaneous syn- or post-orogenic magmatism in the eastern CAOB. We conclude that the early Mesozoic granites in the CAOB were emplaced in a variety of tectonic settings.**

Key words: Mesozoic granite, U-Pb zircon dating, geochemistry, Nd-Hf isotopes, Central Asian Orogenic Belt, Chinese Altai

* Institute of Geology, Chinese Academy of Geological Sciences, Beijing 100037, China
** Beijing SHRIMP Center, Chinese Academy of Geological Sciences, Beijing 100037, China
*** Department of Geosciences, National Taiwan University, and Institute of Earth Sciences, Academia Sinica, Taipei, Taiwan
§ Institute of Precambrian Geology and Geochronology, Russian Academy of Sciences, St. Petersburg 199034, Russian Federation
§§ Department of Applied Geology, Curtin University, G.P.O. Box U1987, Perth 6845 WA, Australia
† Corresponding author: Present address: Institute of Geology, Chinese Academy of Geological Sciences, Baiwanzhuang Road 26, Beijing, 100037, P. R. China; Tel: +86 10 68999732; E-mail: taowang@cags.ac.cn, taowang@pku.edu.cn

INTRODUCTION

The Central Asian Orogenic Belt (CAOB), also known as the Altaid Tectonic Collage (Sengör and others, 1993), evolved over a period of some 800 Ma from *ca.* 1100 Ma to *ca.* 250 Ma. It is the largest Phanerozoic accretionary orogen in the world and the most important site of Phanerozoic crustal growth (for example, Sengör and others, 1993; Wickham and others, 1996; Jahn and others, 2000a, 2000b; Kovalenko and others, 2004). In the last two decades, many studies have been carried out on (1) the early-middle Paleozoic accretionary processes (for example, Coleman, 1989; Windley and others, 2002; Badarch and others, 2002; Kovalenko and others, 2003a; Xiao and others, 2004, 2008, 2009, 2010; Kovach and others, 2013), and (2) the late Paleozoic post-collisional or post-orogenic processes (for example, Yarmolyuk and others, 2002; Han and others, 2010) and tectonic activities (for example, Sengör and others, 1993; Laurent-Charvet and others, 2003). However, an important aspect of post-accretionary or intraplate tectonism and magmatism has not been widely studied. Some research in the last decade has revealed that Mesozoic magmatism occurs extensively in the eastern CAOB, where it is predominantly related to the huge Mongol-Okhotsk suture zone and the Circum-Pacific arcs (for example, Wu and others, 2000; Yarmolyuk and others, 2002; Litvinovsky and others, 2002a, 2002b, 2011; Kovalenko and others, 2003b, 2003c; Yakubchuk, 2004; Jahn and others, 2009). In the central part of the CAOB (for example, Mongolia), Mesozoic magmatism has also been recognized and intensely studied (for example, Yarmolyuk and others, 2002, 2005; Jahn and others, 2004; Wang and others, 2004); and it has been concluded that this magmatism could have occurred in a variety of settings, including post-orogenic, intraplate, or in an active margin related to subduction of the Mongol-Okhotsk Ocean. Recently, Mesozoic magmatism has been recognized from the western part of the CAOB, for example, the Russian Altai (Vladimirov and others, 2001, 2005; Annikova and others, 2006; Pavlova and others, 2008). In the Chinese Altai, available Ar-Ar and K-Ar age data also indicate the existence of Mesozoic granitic intrusions (and pegmatites) and granite-hosted ore deposits (for example, Chen and others, 2000; Wang and others, 2002), even though the occurrence is relatively minor. At present, the Mesozoic magmatism in the western CAOB, including the Chinese Altai, is poorly known in comparison with that in the eastern CAOB. Significantly, the Altai orogen was far away from the Mesozoic oceans, such as the Mongol-Okhotsk Ocean, so that Mesozoic magmatism in this region is likely to be in an intraplate setting. A study of this intraplate magmatism will be helpful in understanding how this can be related to crustal architecture, as well as vertical continental growth after formation of the huge accretionary orogen.

In this work, we address this problem and attempt to establish the geochronological framework for Mesozoic magmatism in the Chinese Altai using U-Pb zircon dating. In addition, we use geochemical and Sr-Nd-Hf isotopic data to evaluate the generation of these granitic rocks. By integrating literature data from the Russian Altai and adjacent areas, we are able to draw some implications for the crustal architecture and continental growth of the entire Altai orogen. The results will enhance our understanding of Mesozoic intraplate anorogenic magmatism in the CAOB: the world's largest Phanerozoic accretionary orogen.

GEOLOGICAL SETTING

The Altai orogen is the major component of the western-central CAOB. It is situated between the Sayan Mountains of southern Siberia to the north and the Junggar Block to the south (fig. 1; for example, Coleman, 1989; Xiao and others, 1992; Parfenov and others, 2004). The Altai orogen extends for more than 2000 km across the national boundaries of China, Mongolia, Russia and Kazakhstan. The orogen comprises several fold-belts (He and others, 1990), which are also referred to as

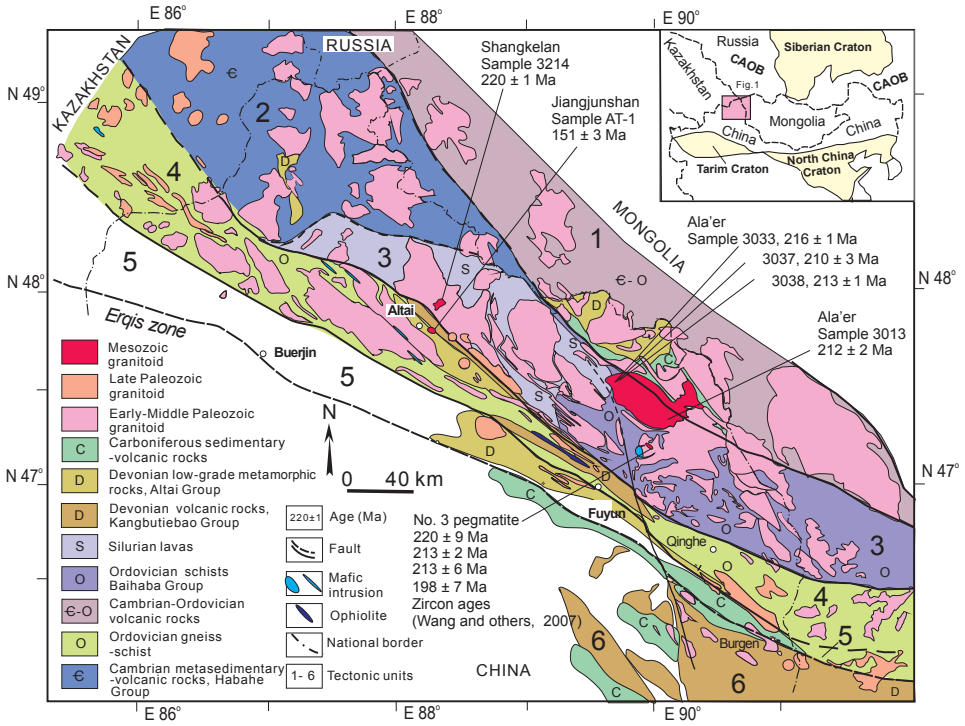

Fig. 1. Generalized geological map of the Chinese Altai orogen, modified from Windley and others (2002), Wang and others (2006) and incorporating our new data. The Mesozoic granitic plutons are named with their U-Pb zircon ages (Ma). Most Paleozoic granitic plutons have been dated by the zircon U-Pb method (Wang and others, 2006). E—Eastern; W—Western; CAOB—Central Asian Orogenic belt.

"terranes" (Badarch and others, 2002; Windley and others, 2002) or "tectonostratigraphic units" (Li and others, 2003; Xiao and others, 2004). According to Windley and others (2002), the Altai orogen in China is composed of the following six terranes (or units, as used here), which are, from north to south (fig. 1):

Unit 1 constitutes the northern part of the Chinese Altai and consists largely of Devonian to Early Carboniferous metavolcanic (andesite and dacite) and metasedimentary rocks.

Units 2 and 3 make up the central part of the Chinese Altai and are an important part of the Altai microcontinent (for example, Windley and others, 2002). Unit 2 consists of Neoproterozoic (Sinian) to Middle Ordovician low-grade metamorphic sedimentary and volcanic rocks (the Habahe Group), with minor Early Devonian sedimentary and volcanic rocks. Unit 3 contains amphibolite- and greenschist-facies metasediments and metavolcanics. According to some workers, Units 2 and 3 may belong to a single tectonic unit (Windley and others, 2002; Li and others, 2003; Xiao and others, 2004).

Units 4 and 5 are located in the southern Chinese Altai. Unit 4 consists predominately of Silurian to Devonian low-grade metamorphic arc-type volcanic rocks. Unit 5 is mainly composed of Devonian fossiliferous successions that are, in turn, overlain by Late Carboniferous formations. Gneisses and schists also occur locally.

Unit 6 is made entirely of Devonian island arc rocks, with a small amount of Ordovician limestones and some Carboniferous island-arc volcanics (Yu and others, 1993). This terrane belongs to the Junggar Block (Kazakhstan plate; fig. 1) and is

separated from the Altai orogen (Unit 5) by the Erqis Fault, one of the largest transcurrent faults in Central Asia (Sengör and others, 1993; He and others, 1994).

The sedimentary and metasedimentary rocks of the Habahe Group in Units 2 and 3 were traditionally considered as the Precambrian basement of the Chinese Altai. However, a recent study on detrital zircon U–Pb ages constrained the maximum depositional age at about 470 Ma. Consequently, the existence of a Precambrian basement in the Altai orogen was questioned (Sun and others, 2008; Long and others, 2010). However, Sr-Nd isotopic mapping of the intrusions in Units 2 and 3 suggested that an old crustal component (*ca.* 1600-1000 Ma) is probably present beneath the dated low-grade metasedimentary rocks (see below and Wang and others, 2009a for details). Wang and others (2009a) argued that the Sr-Nd isotopic signatures could be interpreted as due to partial melting of Early Paleozoic meta-sedimentary rocks that contain old crustal components. Alternatively, the low-grade metasedimentary rocks were underlain by an old crustal component or even a Precambrian basement.

The major orogenic processes in the Chinese Altai took place during the early-middle Paleozoic (500-370 Ma; Windley and others, 2002; Xiao and others, 2004; Wang and others, 2006). Shear along the Erqis Fault (for example, Briggs and others, 2009) and high-grade (granulite facies) metamorphism (for example, Wang and others, 2009b) occurred locally in the southern Altai during the late Paleozoic (290-260 Ma). Paleozoic magmatism occurred mainly in three episodes, at: 460 to 370 Ma, 350 Ma, and 290 to 270 Ma, and it has been intensely studied (for example, Wang and others, 2006; Yuan and others, 2007; Tong and others, 2007, 2012). By contrast, Mesozoic magmatism was poorly understood prior to this study.

CHARACTERISTICS AND SAMPLE DESCRIPTIONS OF THE MESOZOIC GRANITIC PLUTONS IN THE CHINESE ALTAI

Granitic plutons are widespread in the Chinese Altai (fig. 1). Most of them belong to the calc-alkaline series and were emplaced in a syn-orogenic setting during the early-middle Paleozoic (Wang and others, 2006; Yuan and others, 2007). However, some plutons were intruded in a post-orogenic setting during the Late Paleozoic (290-270 Ma; Zou and others, 1988; Wang and others, 2002, 2005; Tong and others, 2006a, 2006b, 2012). Despite the widespread distribution of granites in the Chinese Altai, granitic plutons of Mesozoic age are rare, and new zircon dating has identified only three plutons. Their principal characteristics are described below.

Ala'er Batholith

The Ala'er batholith is one of the largest composite batholiths (>2000 km^2) in the Chinese Altai. It intrudes into a series of amphibolite-facies gneisses of the eastern Chinese Altai (Units 1 and 3; fig. 1). The batholith is predominately composed of porphyritic and massive biotite monzogranite. Porphyritic biotite granite occurs mainly at the southern margin of the intrusion, with phenocrysts of microcline and perthite making up 20 to 60 percent of the rock. The phenocrysts vary in size from 1.5 × 3 to 4 × 7 cm and contain quartz and biotite inclusions. Locally, a fine to medium-grained two-mica granite occurs in the inner part of the batholith and a narrow zone of fine-grained biotite granodiorite is present along its eastern and northern margins (Liu and others, 1997). Mafic enclaves are abundant, particularly at the margins.

Samples of porphyritic and massive biotite monzogranite were collected from the eastern and western parts of this batholith (figs. 1 and 2A). These samples contain variable proportions of large microcline-perthite phenocrysts (5-40%) with lengths from 1.5 to 4 cm. The matrix is composed of microcline, plagioclase (An_{10-30}), quartz and biotite. Accessory minerals include zircon, magnetite, apatite, ilmenite, titanite,

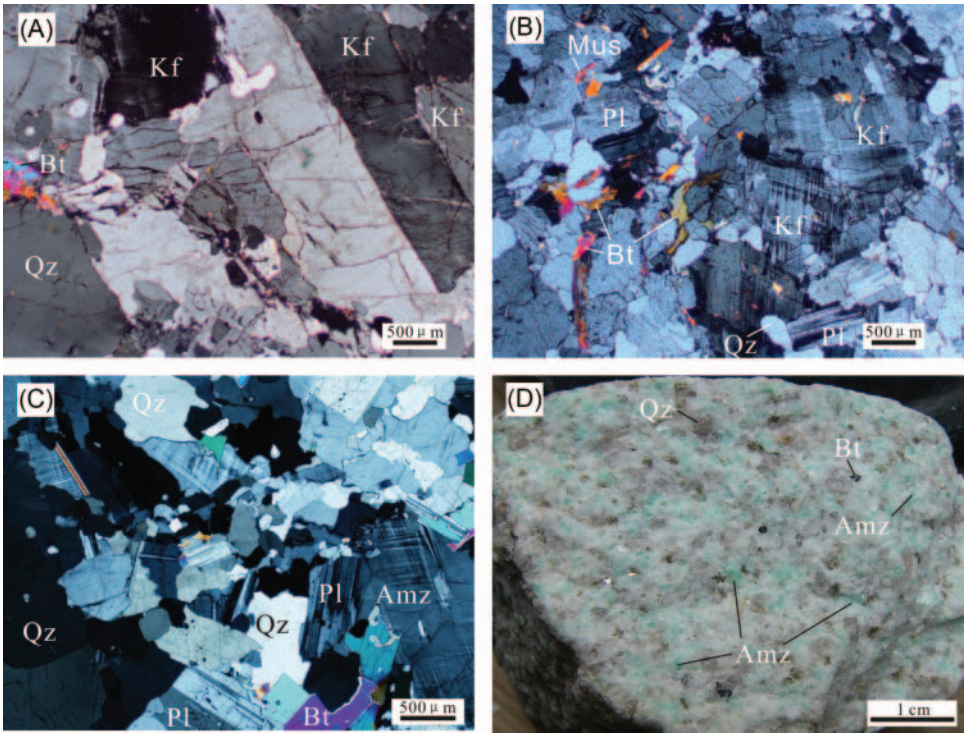

Fig. 2. Photomicrographs of Mesozoic granites in the Chinese Altai. (A) Biotite monzogranite (sample #3028) from the Ala'er batholith, (B) Biotite monzogranite (sample #3214) from the Shangkelan pluton, (C) Amazonite granite (sample #31441) from the Jiangjunshan pluton. The amazonite occurs in microcline-perthite phenocrysts (C) and is green in hand sample (D). Qz: Quartz, Kf: K-feldspar, Pl: Plagioclase, Bt: Biotite, Mus: Muscovite and Amz: Amazonite.

and monazite. Samples #3013, #3033, #3037 and #3038 (fig. 1) were chosen for zircon separation and age determination (table 1A).

Sample #3013 was collected from the southeastern margin of the batholith (fig. 1), about 2.5 km to the north of the Armi'ercala Bridge. The phenocrysts are mainly microcline perthite (30-50% by volume); they are orientated, defining a magmatic flow foliation. Samples #3033, #3037 and #3038 came from the northwestern part of the batholith (fig. 1). Samples (#3013, #3033, #3037 and #3038) are porphyritic biotite granite, medium- to coarse-grained monzogranite, light pink coarse-grained porphyritic biotite monzogranite and light gray coarse-grained biotite monzogranite, respectively (table 1A), and their mineral assemblages are similar, all containing microcline-perthite phenocrysts (10-40%), set in a matrix of plagioclase (10-20%), alkali feldspar (10-15%), quartz (20-30%) and biotite (2-5%).

Shangkelan Pluton

This is a small pluton located about 15 km to the northeast of Altai City (fig. 1). It intrudes the Paleozoic Wuliqi granitic pluton in the central Chinese Altai (Unit 3). The Shangkelan pluton has an irregular shape, with a sharp intrusive contact and a narrow contact metamorphic aureole. Pegmatites with Nb-Ta mineralization occur in the upper part of the pluton and along its contact with the country rocks: no deformation fabrics have been observed. The major rock types comprise albite-rich granite, two-mica monzogranite and biotite monzogranite (see fig. 2B). Samples for the present

TABLE 1A

Zircon U-Pb isotopic data for the Mesozoic granite (Sample 3013) from the Chinese Altai

No.	Size (mm); morphology, type	Wt. (mg)	Pb ppm	U ppm	Isotopic ratios corrected for blank and common Pb $^{206}Pb/^{204}Pb$[a]	$^{207}Pb/^{206}Pb$	$^{208}Pb/^{206}Pb$	$^{207}Pb/^{235}U$	$^{206}Pb/^{238}U$	Rho[b]	Age (Ma) $^{207}Pb/^{235}U$	$^{206}Pb/^{238}U$	$^{207}Pb/^{206}Pb$
1	>100, A30%, 20 gr.	-	U/Pb*	29	965	0.0505±2	0.1271±1	0.2322±12	0.0334±1	0.58	212±1	212±1	216±9
2	-100+85, 50 gr.	0.23	28.4	801	629	0.0505±1	0.0853±1	0.2334±5	0.0335±1	0.62	213±1	213±1	218±4

Notes: all errors are 2 sigma; A30%—abraded zircons, showing percentage–amount of zircon removed during air-abrasion; [a]—measured ratio; [b]—correlation coefficients of $^{207}Pb/^{235}U$ vs. $^{206}Pb/^{238}U$ ratios; [c]—uncertainties (95% confidence level) refer to last digits of corresponding ratios; *—U/Pb ratios for unweighed grains or residues after the acid treatment were determined using the $^{208}Pb/^{235}U$ spike solutions.

TABLE 1B

Zircon U-Pb isotopic data for the Mesozoic granites from the Chinese Altai

spot	U (ppm)	Th (ppm)	Th/U	$^{206}Pb^*$ (ppm)	$^{206}Pb_c$ %	$\frac{^{207}Pb^*}{^{206}Pb^*}$	±%	$\frac{^{207}Pb^*}{^{235}U}$	±%	$\frac{^{206}Pb^*}{^{238}U}$	±%	$\frac{^{206}Pb}{^{238}U}$	±	$\frac{^{207}Pb}{^{206}Pb}$	±
Ala'er pluton (Sample 3037, LA-ICPMS, Biotite monzogranite)															
3037-1	432	106	0.25	73	0.00	0.0516	1.0	0.3002	2.7	0.0422	3.9	267	2	266	10
3037-2	544	199	0.37	86	0.04	0.0516	1.0	0.2448	2.2	0.0344	3.2	218	2	268	10
3037-3	655	87	0.13	188	0.00	0.0511	1.0	0.2336	2.1	0.0332	3.0	210	2	244	10
3037-4	1342	232	0.17	213	0.60	0.0512	1.5	0.2399	3.0	0.0340	3.1	216	2	248	36
3037-5	640	126	0.20	96	0.00	0.0514	1.0	0.2461	2.2	0.0347	3.2	220	2	257	10
3037-6	565	187	0.33	79	0.00	0.0504	1.0	0.2244	2.0	0.0323	2.9	205	2	213	10

Table 1B
(continued)

spot	U (ppm)	Th (ppm)	Th/U	$^{206}Pb^*$ (ppm)	$^{206}Pb_c$ %	$\frac{^{207}Pb^*}{^{206}Pb^*}$	±%	$\frac{^{207}Pb^*}{^{235}U}$	±%	$\frac{^{206}Pb^*}{^{238}U}$	±%	$\frac{^{206}Pb}{^{238}U}$	±	$\frac{^{207}Pb}{^{206}Pb}$	±
Ala'er pluton (Sample 3037, LA-ICPMS, Biotite monzogranite)															
3037-1	432	106	0.25	73	0.00	0.0516	1.0	0.3002	2.7	0.0422	3.9	267	2	266	10
3037-8	394	302	0.77	56	0.00	0.0566	1.0	0.2515	2.3	0.0322	2.9	205	2	475	9
3037-9	650	112	0.17	170	0.00	0.0615	1.0	0.2636	2.4	0.0311	2.8	197	2	658	9
3037-10	889	170	0.19	138	0.69	0.0501	1.6	0.2285	3.0	0.0331	3.0	210	2	197	38
3037-11	815	97	0.12	117	0.00	0.0503	1.0	0.2292	2.1	0.0330	3.0	209	2	210	10
3037-12	1382	156	0.11	198	0.36	0.0501	1.4	0.2335	2.6	0.0338	3.1	214	2	199	34
3037-13	263	424	1.61	42	1.24	0.0553	4.7	0.2326	10.6	0.0305	3.4	194	2	423	108
3037-14	1158	1259	1.09	375	0.00	0.0563	1.0	0.5767	5.1	0.0743	6.7	462	4	463	9
3037-15	184	224	1.22	26	0.09	0.0562	1.0	0.2575	2.3	0.0332	3.0	211	2	459	9
3037-16	328	126	0.38	71	0.00	0.0541	1.0	0.3698	3.3	0.0495	4.5	312	3	376	9
3037-17	708	80	0.11	99	0.00	0.0579	1.0	0.2646	2.4	0.0331	3.0	210	2	526	9
3037-18	1835	210	0.11	258	0.00	0.0542	1.0	0.2445	2.2	0.0327	2.9	207	2	378	9
3037-19	939	794	0.85	133	0.00	0.0505	1.0	0.2356	2.1	0.0338	3.0	214	2	218	9
3037-20	1857	189	0.10	245	0.00	0.0739	1.0	0.3290	2.9	0.0323	2.9	205	2	1038	8
Ala'er pluton (Sample 3033, LA-ICPMS, Medium-coarse-grained biotite monzogranite)															
3033-1	347	312	0.90	13		0.0524	3.7	0.2447	3.7	0.0339	1.7	215	4	304	84
3033-2	594	294	0.49	21		0.0525	2.9	0.2489	2.9	0.0344	1.7	218	4	307	65
3033-3	296	366	1.24	12		0.0546	5.4	0.2567	5.5	0.0341	1.9	216	4	396	121
3033-4	971	321	0.33	33		0.0509	1.6	0.2397	1.6	0.0341	1.7	216	4	238	38
3033-5	2726	49	0.02	85		0.0504	1.1	0.2378	1.2	0.0342	1.7	217	4	214	26
3033-6	1366	373	0.27	53		0.0519	1.3	0.2855	1.4	0.0399	1.8	252	5	281	30
3033-7	1888	68	0.04	59		0.0512	1.2	0.2407	1.2	0.0341	1.7	216	4	249	27
3033-8	969	90	0.09	36		0.0529	1.6	0.2890	1.6	0.0396	1.7	251	4	323	36
3033-9	1320	226	0.17	43		0.0513	1.3	0.2444	1.4	0.0345	1.7	219	4	255	30
3033-10	1419	79	0.06	45		0.0548	2.4	0.2581	2.4	0.0341	1.7	216	4	406	54
3033-11	347	330	0.95	13		0.0520	3.7	0.2433	3.7	0.0339	1.7	215	4	284	84
3033-12	1208	371	0.31	41		0.0509	1.8	0.2418	1.9	0.0344	1.7	218	4	239	42
3033-13	2205	836	0.38	74		0.0504	1.4	0.2367	1.5	0.0341	1.9	216	4	213	31

Table 1B
(continued)

spot	U (ppm)	Th (ppm)	Th/U	$^{206}Pb^*$ (ppm)	$^{206}Pb_c$ %	$\frac{^{207}Pb^*}{^{206}Pb^*}$	±%	$\frac{^{207}Pb^*}{^{235}U}$	±%	$\frac{^{206}Pb^*}{^{238}U}$	±%	$\frac{^{206}Pb}{^{238}U}$	±	$\frac{^{207}Pb}{^{206}Pb}$	±
Ala'er pluton (Sample 3033, LA-ICPMS, Medium-coarse-grained biotite monzogranite)															
3033-14	1510	353	0.23	50		0.0511	1.5	0.2421	1.5	0.0344	1.7	218	4	246	34
3033-15	1404	266	0.19	45		0.0510	1.4	0.2385	1.4	0.0339	1.7	215	4	241	32
3033-16	1133	572	0.50	39		0.0526	1.3	0.2450	1.4	0.0337	1.7	214	4	314	31
3033-17	1082	68	0.06	34		0.0554	2.2	0.2604	2.2	0.0341	1.7	216	4	430	48
3033-18	876	302	0.34	29		0.0509	1.6	0.2362	1.7	0.0336	1.7	213	4	238	37
3033-19	2956	190	0.06	93		0.0504	1.1	0.2374	1.2	0.0341	1.7	216	4	216	26
3033-20	1288	241	0.19	42		0.0530	1.3	0.2517	1.4	0.0345	1.7	218	4	328	31
3033-21	1534	172	0.11	49		0.0508	1.5	0.2402	1.6	0.0343	1.8	217	4	232	34
3033-22	1264	749	0.59	44		0.0505	1.6	0.2374	1.6	0.0341	1.7	216	4	219	36
3033-23	245	376	1.53	10		0.0532	4.5	0.2498	4.5	0.0341	1.8	216	4	336	101
3033-24	545	307	0.56	19		0.0518	2.2	0.2442	2.3	0.0342	2.0	217	4	277	51
3033-25	899	280	0.31	30		0.0515	1.8	0.2422	1.8	0.0341	1.7	216	4	263	41
3033-26	594	292	0.49	21		0.0513	2.8	0.2443	2.9	0.0346	1.7	219	4	253	66
3033-27	904	193	0.21	35		0.0504	2.2	0.2808	2.6	0.0404	1.8	255	5	214	52
3033-28	1543	7444	4.83	89		0.0529	1.8	0.2482	1.9	0.0340	1.9	216	4	325	40
3033-29	788	150	0.19	31		0.0509	3.4	0.2792	3.5	0.0398	1.8	251	4	237	79
3033-30	503	438	0.87	19		0.0527	3.3	0.2478	3.5	0.0341	1.8	216	4	315	75
Ala'er pluton(Sample 3038, LA-ICPMS, Porphyritic biotite monzogranite)															
3038-1	899	393	0.44	31		0.0542	2.1	0.2492	2.2	0.0333	0.8	211	2	380	48
3038-2	1170	740	0.63	43		0.0525	1.9	0.2424	2.0	0.0335	0.8	212	2	309	44
3038-3	2185	167	0.08	68		0.0517	1.6	0.2383	1.7	0.0334	0.8	212	2	273	36
3038-4	1459	452	0.31	48		0.0506	1.8	0.2325	1.8	0.0333	0.8	211	2	223	42
3038-5	2121	48	0.02	65		0.0517	1.5	0.2373	1.6	0.0333	0.8	211	2	271	35
3038-6	1329	393	0.30	44		0.0532	1.8	0.2463	1.9	0.0336	0.8	213	2	336	42
3038-7	2293	176	0.08	71		0.0515	1.4	0.2380	1.5	0.0335	0.8	213	2	262	33
3038-8	958	730	0.76	36		0.0514	2.1	0.2391	2.2	0.0337	0.8	214	2	259	48
3038-9	2854	176	0.06	88		0.0509	1.4	0.2355	1.4	0.0336	0.8	213	2	235	32
3038-10	1493	403	0.27	49		0.0505	1.6	0.2324	1.6	0.0334	0.8	212	2	218	36
3038-11	2286	238	0.10	71		0.0504	1.4	0.2316	1.5	0.0333	0.8	211	2	215	33

Table 1B
(continued)

spot	U (ppm)	Th (ppm)	Th/U	$^{206}Pb^*$ (ppm)	$^{206}Pb_c$ %	$\frac{^{207}Pb^*}{^{206}Pb^*}$	±%	$\frac{^{207}Pb^*}{^{235}U}$	±%	$\frac{^{206}Pb^*}{^{238}U}$	±%	$\frac{^{206}Pb}{^{238}U}$	±	$\frac{^{207}Pb}{^{206}Pb}$	±
Ala'er pluton(Sample 3038, LA-ICPMS, Porphyritic biotite monzogranite)															
3038-15	1446	91	0.06	45		0.0502	1.7	0.2344	1.8	0.0339	0.8	215	2	203	39
3038-16	2499	290	0.12	78		0.0505	1.5	0.2321	1.5	0.0333	0.8	211	2	219	34
3038-17	591	570	0.96	23		0.0537	2.8	0.2484	2.9	0.0336	0.9	213	2	359	64
3038-18	3066	84	0.03	94		0.0509	1.4	0.2343	1.5	0.0334	0.8	212	2	238	33
3038-19	2442	571	0.23	80		0.0505	1.5	0.2343	1.5	0.0336	0.8	213	2	219	34
3038-20	2379	149	0.06	74		0.0504	1.4	0.2319	1.5	0.0334	0.8	212	2	212	34
3038-21	2493	103	0.04	77		0.0499	1.5	0.2320	1.5	0.0337	0.9	214	2	189	34
3038-22	1200	324	0.27	40		0.0509	2.0	0.2372	2.1	0.0338	0.8	214	2	236	46
3038-23	3126	68	0.02	95		0.0503	1.4	0.2310	1.4	0.0333	0.8	211	2	207	32
3038-24	4297	434	0.10	136		0.0507	1.3	0.2363	1.4	0.0338	0.8	214	2	227	31
3038-25	2738	336	0.12	86		0.0508	1.4	0.2342	1.5	0.0335	0.8	212	2	230	32
3038-26	3401	193	0.06	106		0.0502	1.4	0.2336	1.4	0.0338	0.8	214	2	204	32
3038-27	3503	498	0.14	112		0.0509	1.3	0.2366	1.4	0.0337	0.8	214	2	235	31
3038-28	1967	152	0.08	61		0.0504	1.5	0.2312	1.5	0.0333	0.8	211	2	211	34
3038-29	995	373	0.37	34		0.0528	2.0	0.2465	2.1	0.0339	0.8	215	2	320	46
Shangkelan pluton (Sample 3214, SHRIMP, Biotite monzogranite)															
3214.1	192	131	0.71	6	1.09	0.0447	7.2	0.2050	7.7	0.0333	2.6	211	5	-70	180
3214.2	845	261	0.32	23	0.12	0.0515	3.0	0.2268	3.7	0.0319	2.2	203	4	265	68
3214.3	174	92	0.54	5	0.00	0.0488	6.0	0.2130	6.6	0.0316	2.7	201	5	139	140
3214.4	876	423	0.50	19	1.57	0.0558	7.1	0.1910	7.4	0.0249	2.2	158	3	443	160
3214.5	444	636	1.48	12	0.58	0.0510	5.6	0.2210	6.3	0.0314	2.9	200	6	243	130
3214.6	76	120	1.63	2	0.00	0.0577	7.8	0.2720	9.2	0.0342	4.9	217	11	520	170
3214.7	1552	1005	0.67	39	4.07	0.0465	9.8	0.1820	10.0	0.0284	2.1	180	4	24	240
3214.8	713	639	0.93	20	0.12	0.0467	3.1	0.2088	3.9	0.0325	2.5	206	5	32	74
3214.9	313	373	1.23	8	0.00	0.0487	4.2	0.2074	4.8	0.0309	2.3	196	6	134	98
3214.10	871	489	0.58	21	0.32	0.0457	3.4	0.1766	4.0	0.0280	2.1	178	4	-18	81
3214.11	314	178	0.58	8	0.44	0.0500	6.2	0.2120	6.6	0.0308	2.3	196	5	196	140
3214.12	742	416	0.58	21	0.18	0.0505	3.0	0.2262	3.7	0.0325	2.1	206	4	219	69

TABLE 1B
(continued)

spot	U (ppm)	Th (ppm)	Th/U	$^{206}Pb^*$ (ppm)	$^{206}Pb_c$ %	$\frac{^{207}Pb^*}{^{206}Pb^*}$	±%	$\frac{^{207}Pb^*}{^{235}U}$	±%	$\frac{^{206}Pb^*}{^{238}U}$	±%	$\frac{^{206}Pb}{^{238}U}$	±	$\frac{^{207}Pb}{^{206}Pb}$	±
Jiangjunshan pluton (Sample AT1, SHRIMP, Two mica monzogranite)															
3038-15	1446	91	0.06	45		0.0502	1.7	0.2344	1.8	0.0339	0.8	215	2	203	39
AT1-1	1567	1732	1.11	46	0.00	0.0509	1.7	0.1700	4.0	0.0243	4.0	155	3	236	39
AT1-2	507	931	1.83	17	0.00	0.0493	2.4	0.1620	5.0	0.0239	5.0	152	3	164	55
AT1-3	137	198	1.44	4	0.00	0.0533	4.4	0.1770	9.0	0.0241	5.0	153	3	343	98
AT1-4	827	535	0.65	21	0.01	0.0497	3.3	0.1630	6.0	0.0237	4.0	151	3	181	76
AT1-5	695	403	0.58	17	0.00	0.0505	3.1	0.1560	6.0	0.0225	4.0	143	3	217	72
AT1-6	752	843	1.12	22	0.11	0.0488	6.6	0.1580	11.0	0.0235	5.0	150	3	140	147
AT1-7	399	386	0.97	11	0.00	0.0520	2.5	0.1760	6.0	0.0246	5.0	157	3	284	57
AT1-8	421	265	0.63	11	0.00	0.0482	0.3	0.1620	6.0	0.0244	5.0	155	3	107	60
AT1-9	514	689	1.34	16	0.00	0.0518	2.9	0.1710	6.0	0.0239	5.0	152	3	278	66
AT1-10	357	162	0.45	9	0.04	0.0481	4.7	0.1520	8.0	0.0229	5.0	146	3	107	108
AT1-11	618	405	0.65	16	0.00	0.0492	2.0	0.1590	5.0	0.0234	4.0	149	3	155	47
AT1-12	217	136	0.62	5	0.03	0.0452	7.2	0.1440	11.0	0.0232	5.0	148	3	0	120
AT1-13	429	229	0.53	11	0.04	0.0479	4.4	0.1530	8.0	0.0232	4.0	148	3	96	100

Sample 3214 was dated at the Beijing SHRIMP Center; Errors are 1-sigma; Pb_c and Pb* indicate the common and radiogenic portions, respectively; Pb_c corrected using measured ^{204}Pb. Sample AT1 was dated at Curtin University, Australia; * corrected.

Sample 3037 was analyzed at the Key Laboratory of Continental Dynamics of the Northwest University, Xi'an, China.

Samples 3033, 3038, 3213, 3150 were analyzed at the Tianjin Institute of Mineral Resources.

study came from the central and western parts of the pluton, on the road west of the Kelan River. They are medium-grained monzogranite and alkali feldspar granite, and are composed of plagioclase (20-25%), alkali feldspar (30-45%), quartz (30-35%), biotite (5%) and muscovite (3%). Sample #3214, was obtained from a medium-grained biotite monzogranite, was selected for zircon separation and U-Pb geochronology.

Jiangjunshan Pluton

This pluton is located 10 km east-southeast of Altai City (fig. 1). It intrudes a series of Devonian metavolcanic and metasedimentary rocks (the Altai Group) of Unit 4. It has a sharp contact and is devoid of deformation fabrics. The pluton also intrudes a small gabbro body that has been dated at 280 ± 6 Ma by zircon U-Pb SHRIMP analysis (T. Wang, unpublished data).

The rock types include alkali feldspar granite, two-mica monzogranite, garnet-bearing muscovite monzogranite and biotite monzogranite. The mineral assemblage of biotite monzogranite (sample #3148) comprises plagioclase (25-30%), alkali feldspar (30-35%), quartz (20-25%) and biotite (7%). Garnet-bearing muscovite monzogranite (sample #3143) is composed of alkali feldspar (25-35%), quartz (25-30%), plagioclase (30-35%), muscovite (5%), and minor garnet (1%). Some granitic rocks, for example samples #31441 and A5051, contain amazonite (figs. 2C and 2D). Accessory minerals are zircon, magnetite, apatite, titanite, and monazite. In addition, amazonite-bearing granitic veins cut the pluton, and locally the veins contain Be, Nb and Ta mineralization. Sample AT-1 is a two mica monzogranite (A-type granite), composed of plagioclase (25-30%), alkali feldspar (35-40%), quartz (20-25%), biotite (3%) and muscovite (2%). It was chosen for U-Pb zircon dating.

U-Pb ZIRCON GEOCHRONOLOGY

The zircon grains separated from the above samples are colorless, yellow or light brown, transparent and commonly euhedral. The grain sizes range from 50 to 600 μm along the c-axis with a length/width ratio of 2:1 to 7:1. Almost all grains have concentric oscillatory zoning (fig. 3), suggesting a magmatic origin. However, some grains are more complex (especially in sample #3037 from the Ala'er batholith) and show evidence of recrystallization. The zircon U-Pb isotopic analyses were performed using SHRIMP II (Sensitive High Resolution Ion MicroProbe) at the Beijing SHRIMP Center, China, and at Curtin University, Australia; by LA-ICPMS at the Key Laboratory of Continental Dynamics of the Northwest University, Xi'an, and at the Tianjin Institute of Geology and Mineral Resources, Tianjin, China, and by TIMS (Thermal Ionization Mass Spectrometry) at the Institute of Precambrian Geology and Geochronology (IPGG), Russian Academy of Sciences, St. Petersburg (see details in the Appendix).

Age Data for the Ala'er Batholith

Sample #3013.—Zircon grains from sample #3013 were dated using TIMS (table 1A and fig. 4A). Twenty abraded grains (Krogh, 1982) from size fraction >100 μm (analysis 1, table 1A) and fifty unabraded clean grains from the 85 to 100 μm fraction (analysis 2, table 1A) were analyzed as two separate multigrain fractions. The data points are concordant at 212 ± 2 Ma (MSWD =1.6; fig. 4A). Since the analysed zircon grains are of magmatic origin, this age is interpreted as the time of zircon crystallization and, therefore, the emplacement age of the granite.

Sample #3037.—Zircon grains from sample #3037 were analyzed using LA-ICPMS and a total of 19 sites were investigated (table 1B). The 14 most concordant data-points on oscillatory zoned domains (fig. 4B) yield a weighted mean $^{206}Pb/^{238}U$ age of 211 ± 3 Ma (MSWD = 5.8), which is identical to that of sample #3013. Likewise, this age is interpreted as the time of zircon crystallization and granite emplacement. Note that

Fig. 3. Cathodoluminescence (CL) images of selected dated zircon grains from samples #3013, #3033, #3038 and #3214, and scanning electron microscope backscatter (BSE) images of sample #3037 from the granites in the Chinese Altai. Analyzed spots are circled, and numbers refer to U-Pb ages presented in table 1.

among these data, six discordant points give an apparent $^{206}Pb/^{238}U$ age of ~205 Ma (fig. 4B). The significance of this date is unclear. However, we notice that the data have an unusual ^{204}Pb correction, possibly resulting from a post-magmatic isotopic disturbance. The 4 remaining data points show scattered $^{206}Pb/^{238}U$ dates from 270, 340 to 520 Ma (table 1B). These zircon grains are considered to be xenocrysts.

Sample #3033.—A total of thirty spots were analyzed using LA-ICP-MS. Twenty six data points on oscillatory zoned domains (fig. 4C) are tightly grouped on the concordia diagram, and yield a weighted mean $^{206}Pb/^{238}U$ age of 216 ±1 Ma with MSWD = 0.6. The zircon domains have U and Th concentrations of 296 to 2956 ppm and 49 to 836 ppm, respectively (table 1B). This age is interpreted as the time of zircon crystallization in the granite. The other 4 analyses on zircon grains with rounded cores and U and Th concentrations of 788 to 1366 ppm and 90 to 373 ppm, respectively, (table 1B) record ages ranging from 255 to 251 Ma: these grains are interpreted as xenocrysts.

Sample #3038.—Twenty-nine spots on zircons with the oscillatory zoning (fig. 3D) were analyzed using LA-ICP-MS and the results yielded a tight cluster of near-

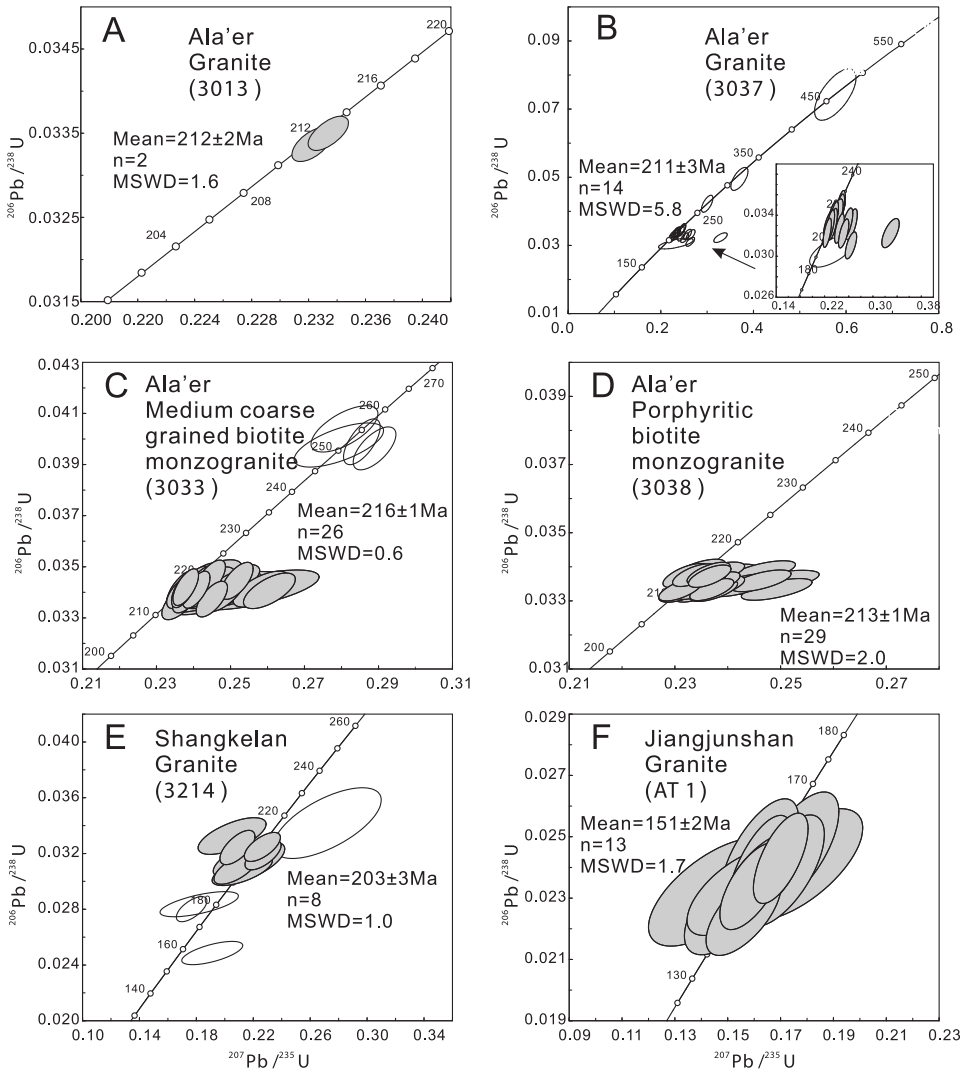

Fig. 4. U-Pb concordia diagrams of zircon data obtained by TIMS (A), LA-ICPMS (B, C and D) and SHRIMP (E and F) for the Ala'er (samples #3013, #3033, #3037 and #3088), Shangkelan (#3214) and Jiangjunshan (AT-1) intrusions. The data used for age calculation are shown in gray.

concordant data points, which give an age of 213 ± 1 Ma with MSWD = 2.0 (fig. 4D). The U and Th concentrations of the analyzed spots range from 591 to 4297 ppm and 48 to 740 ppm, respectively (table 1B). We interpret this as the crystallization age of the granite.

Age Data for the Shangkelan Pluton

Sample #3214.—U-Pb isotopic analyses of zircon from sample #3214 were performed using the SHRIMP II at the Beijing SHRIMP Center. Twelve spots were analyzed (table 1B), and the eight most concordant points on domains with oscillatory zoning define a weighted mean $^{206}Pb/^{238}U$ age of 203 ± 3 Ma with MSWD = 1.0 (fig.

4E). This age is interpreted as the time of zircon crystallization and emplacement of the pluton. The remaining data points are scattered, and their significance is not clear. Three data points are younger but more discordant, with two giving $^{206}Pb/^{238}U$ ages of ~180 Ma and another an age of ~158 Ma, all of which might have resulted from post-magmatic Pb loss.

Age Data for the Jiangjunshan Pluton

Sample AT-1.—Zircon grains from sample AT-1 were analyzed by SHRIMP II at Curtin University, Australia. Thirteen analyses from 13 zircon grains are concordant or near-concordant, and define a $^{206}Pb/^{238}U$ age of 151 ± 3 Ma (fig. 4F). This age is considered as the emplacement time of the pluton.

CHEMICAL AND ISOTOPIC (Nb, Sr, Hf) ANALYSES

The procedures for the analysis of major oxides and trace element abundances, Nd-Sr isotope compositions and *in-situ* zircon Lu-Hf isotope compositions are given in the Appendix.

Major and Trace Elements

Major and trace element data are presented in table 2. The granites are highly siliceous (SiO_2 = 70-78 wt.%), except for sample #5945 (65 wt.%), and have high alkali contents (Na_2O = 2.5 − 6.0 wt.%, K_2O = 3.0 − 6.4 wt.%) but have very low "cafemic" oxide contents (table 2). Al_2O_3 ranges from 12.0 to 16.0 weight percent (except 20 wt.% for sample #5045). The Ala'er granites show very high K_2O contents and K_2O/Na_2O ratios (>1.5) with SiO_2 of 71 to 73 weight percent. This feature is typical of the shoshonitic series (fig. 5A; Peccerillo and Taylor, 1976; Väisänen and others, 2000) and even the super-shoshonitic series (K_2O/Na_2O>2) (Turner and others, 1996). By contrast, most of the Jiangjunshan and Shangkelan granite samples follow the high-K calc-alkaline trends in the K_2O vs. SiO_2 diagram (fig. 5A), although two samples of the Jiangjunshan pluton are shoshonitic. These granites are weakly peraluminous (A/NCK=1.0-1.4, table 2; fig. 5B) and exhibit highly differentiated calc-alkaline features (fig. 5C).

The Ala'er granites exhibit highly fractionated REE patterns with LREE abundances >100 x, HREE <10 x chondrite, and strong negative Eu anomalies (fig. 6A). The Shangkelan granites also show fractionated REE patterns with strong negative Eu anomalies (fig. 6C). The Jiangjunshan granites show two types of REE patterns (fig. 6E). The first type is similar to that of the Shangkelan granites, and the dominant second type is characterized by low LREE (<60 x chondrite) and high HREE abundances (> 50 x chondrite), with very large negative Eu anomalies. The lanthanide tetrad effect is demonstrated in these samples, which is corroborated by the high K/Ba, low Nd/Ta and low Zr/Hf ratios (Bau, 1996; Irber, 1999; Jahn and others, 2001, 2004).

In the spidergrams, all the samples show negative anomalies of Ba, Nb, Ta, Sr, P, Eu and Ti, and positive Th and Nd anomalies (figs. 6B, 6D, and 6F). Such anomalies are most pronounced in the Jiangjunshan granites.

Whole-Rock Sr-Nd Isotopes

Sr-Nd isotopic data for 11 samples are shown in table 3. The age-corrected initial Sr isotope ratios (I_{Sr}) of the Ala'er granites range from 0.7065 to 0.7129. Some calculated I_{Sr} values for the Shangkelan and Jiangjunshan granites are unusually low (<0.70) or exceptionally high (>0.72). These values do not have any petrogenetic significance because they were obtained with very large corrections in the radiogenic $^{87}Sr/^{86}Sr$ ratios due to extremely high Rb/Sr ratios (table 3). The ε_{Nd} (210 Ma) values of the Ala'er and Shangkelan granites are negative (−0.7 to −3.9). By contrast, the Jiangjunshan granites have positive ε_{Nd} (151 Ma) values (+1.0 to +5.2) (fig. 7A). The

TABLE 2

Chemical compositions of the Mesozoic granites from the Chinese Altai

Pluton	**Ala'er**					**Shangkelan**	
Name							
Sample No.	**3013**	**3014**	**3028**	**3033**	**3037**	**3212**	**3214**
Rock type	Porphyr. biotite granite	Grano-diorite	Biotite monzogranite	Monzogranite	Biotite monzogranite	Two-mica granite	Biotite monzogranite
	Major elements (in wt %)						
SiO_2	70.47	72.17	73.06	73.06	72.37	73.77	75.68
TiO_2	0.46	0.24	0.18	0.27	0.20	0.22	0.11
Al_2O_3	14.55	13.73	14.77	14.24	14.55	13.91	13.38
Fe_2O_3	0.81	0.99	0.32	0.38	0.44	1.12	0.27
FeO	1.31	1.28	0.99	1.19	1.00	0.39	0.47
MnO	0.04	0.03	0.02	0.02	0.02	0.04	0.04
MgO	0.60	0.52	0.47	0.52	0.44	0.26	0.22
CaO	1.53	0.93	0.94	1.09	1.06	0.44	0.08
Na_2O	3.00	2.53	3.18	2.93	2.81	4.50	3.76
K_2O	6.28	6.36	5.55	5.66	6.16	4.22	4.74
P_2O_5	0.24	0.12	0.19	0.29	0.35	0.07	0.03
H_2O^+	0.22	0.48	0.54	0.42	0.46	0.66	0.50
LOI	0.32	0.46	0.57	0.37	0.46	0.68	0.65
Total	99.8	99.8	100.8	100.4	100.3	100.3	99.9
A/NCK	1.00	1.08	1.14	1.10	1.10	1.09	1.17
	Trace elements (in ppm)						
La	88.0	138	36.9	49.2	35.1	85.3	46.5
Ce	172	276	76.2	101	73.2	159	80.3
Pr	20.2	32.4	8.77	12.2	8.53	16.8	8.15
Nd	70.7	118	32.8	42.5	31.5	54.7	26.1
Sm	13.1	21.3	6.71	9.07	7.54	10.3	5.49
Eu	2.21	2.34	0.69	0.92	0.91	1.00	0.58
Gd	8.18	12.7	4.10	5.27	5.24	6.17	4.25
Tb	1.16	1.59	0.60	0.73	0.80	1.06	0.91
Dy	5.73	7.15	2.84	3.66	4.28	6.01	6.09
Ho	0.96	1.02	0.45	0.60	0.74	1.18	1.26
Er	2.52	2.46	1.09	1.59	2.13	3.70	4.28
Tm	0.31	0.23	0.13	0.21	0.29	0.61	0.78
Yb	1.84	1.18	0.77	1.24	1.81	4.56	6.37
Lu	0.28	0.18	0.11	0.20	0.26	0.80	1.13
Y	21.9	23.2	10.8	14.1	19.1	30.9	40.7
Total REE	409	638	183	242	191	382	233
δEu	0.61	0.40	0.37	0.37	0.42	0.35	0.35
(La/Yb)N	32	79	32	27	13	13	5
Co	3.57	3.26	2.18	2.91	2.60	1.46	0.17
Ni	4.00	1.74	3.95	5.08	4.41	2.27	0.82
V	30.0	21.7	15.8	24.1	20.1	10.8	6.8
Th	38.9	87.0	27.5	35.1	22.9	46.3	29.0
Rb	187	186	194	288	248	390	348
Sr	274	297	87.2	107	127	83.6	52.7
Ba	612	1029	232	347	387	171	152
Cs	3.84	3.30	8.34	5.52	4.55	8.77	4.71
Ta	1.13	0.47	0.96	2.15	0.98	5.96	6.62
Nb	17.2	8.34	9.15	18.4	13.3	59.0	62.3
Hf	9.47	2.80	4.42	5.79	5.03	8.01	5.59
Zr	354	110	123	166	147	168	102
Ga	21.9	22.1	21.6	23.8	22.3	35.1	37.1
Sc	5.53	4.19	2.90	3.20	2.70	9.41	11.3
U	1.11	2.32	5.53	4.86	4.35	6.53	10.0

TABLE 2
(continued)

Pluton Name	**Shangkelan**			**Jiangjunshan**			
Sample No.	**3211**	**32112**	**XSK-2***	**3143**	**3148**	**3150**	**3141-A**
Rock type	Biotite monzogranite	Two-mica granite	Granite	Two-mica granite	Porphyritic biotite granite	Biotite granite	Two-mica granite
	Major elements (in wt %)						
SiO_2	74.55	76.06	73.87	75.98	73.38	77.05	76.38
TiO_2	0.22	0.10	0.08	0.01	0.27	0.01	<0.01
Al_2O_3	13.32	12.98	14.31	13.93	13.45	12.86	13.45
Fe_2O_3	0.58	0.60	0.28	0.18	0.37	0.03	0.23
FeO	1.15	1.19	0.54	0.46	1.65	0.48	0.45
MnO	0.24	0.10	0.05	0.01	0.05	0.01	0.04
MgO	0.29	0.56	0.12	0.02	0.52	0.04	0.01
CaO	0.06	0.03	0.05	0.28	1.31	0.40	0.25
Na_2O	2.80	3.41	5.45	5.33	3.41	4.95	4.25
K_2O	5.16	3.02	4.17	3.04	4.24	3.26	4.10
P_2O_5	0.04	0.03	0.19	0.01	0.23	<0.01	0.02
H_2O^+				0.58	0.46	0.28	
LOI	1.4	1.7	0.65	0.58	0.54	0.33	0.8
Total	99.8	99.8	99.8	100.4	99.9	99.7	100.0
A/NCK	1.29	1.45	1.05	1.11	1.07	1.04	1.13
	Trace elements (in ppm)						
La	85.3	46.5	69.0	87.1	27.0	12.9	5.6
Ce	159	80.3	131.1	146.1	45.2	27.5	17.9
Pr	16.8	8.15	14.6	14.2	5.82	4.58	2.47
Nd	54.7	26.1	51.7	44.9	15.7	21.2	12.6
Sm	10.3	5.49	8.64	6.41	3.44	11.7	5.89
Eu	1.00	0.58	0.69	0.55	0.23	0.04	0.02
Gd	6.17	4.25	6.30	3.58	1.76	16.6	10.2
Tb	1.06	0.91	0.88	0.36	0.32	3.95	2.27
Dy	6.01	6.09	5.63	1.71	1.24	27.9	18.7
Ho	1.18	1.26	0.92	0.18	0.25	6.15	3.89
Er	3.70	4.28	3.22	0.50	0.81	19.1	13.59
Tm	0.61	0.78	0.57	0.06	0.18	3.04	2.38
Yb	4.56	6.37	4.36	0.68	1.35	19.5	16.86
Lu	0.80	1.13	0.73	0.10	0.21	2.93	2.60
Y	30.9	40.7	37.7	6.5		163	135
Total REE	382	233	336	313	103	340	250
δEu	0.35	0.35	0.27	0.32	0.25	0.01	0.01
(La/Yb)N	13	5	11	87	14	0.45	0.22
Co	1.46	0.17	0.40	<0.2		0.11	<0.2
Ni	2.27	0.82	0.80	3.20		0.62	3.10
V	10.8	6.8	12	17		<1.00	<8
Th	46.3	29.0	37.8	47.7		31.1	23.9
Rb	390	348	528	446		279	534
Sr	83.6	52.7	248	57.7		5.31	2.10
Ba	171	152	193	912		3.09	<1
Cs	8.77	4.71	8.20	6.40		7.74	42.0
Ta	5.96	6.62	8.60	4.70		5.61	6.30
Nb	59.0	62.3	87.1	57.4		21.8	17.4
Hf	8.01	5.59	7.30	4.00		5.98	6.60
Zr	168	102	184	63.4		74.6	60.6
Ga	35.1	37.1	33.5	36.1		36.5	35.9
Sc	9.41	11.3	16	20		1.95	2.0
U	6.53	10.0	5.9	6.50		2.59	2.20

TABLE 2
(continued)

Pluton Name	**Jiangjunshan**						
Sample No.	**3141-B**	**3142**	**3146**	**AT-1**	**AT-2**	**A5043**	**A5045**
Rock type	Two-mica granite	Two-mica granite	Amazonite granite	Two-mica monzogranite	Two-mica monzogranite	Granite (main body)	Differentiated granite
	Major elements (in wt %)						
SiO_2	76.61	76.19	77.98	78.10	73.54	73.73	64.58
TiO_2	<0.01	<0.01	<0.01	0.04	0.08	0.02	0.02
Al_2O_3	13.26	13.57	12.54	12.02	14.37	14.94	20.57
Fe_2O_3	0.25	0.13	0.11	0.28	0.96	0.15	0.08
FeO	0.51	0.26	0.21	0.31	0.23	0.34	0.35
MnO	0.03	0.02	<0.01	0.01	0.03	0.03	0.02
MgO	0.02	0.01	0.02	0.01	0.28	0.00	0.00
CaO	0.33	0.50	0.14	0.42	0.84	0.60	0.45
Na_2O	4.12	4.69	3.49	3.71	3.62	4.66	6.06
K_2O	4.02	3.76	4.76	4.03	4.74	3.87	5.96
P_2O_5	<0.01	<0.01	<0.01	0.04	0.19	0.00	0.00
H_2O^+							
LOI	0.8	0.8	0.7	0.85	0.90	0.68	0.46
Total	100.0	99.9	100.0	99.8	99.8	99.02	98.55
A/NCK	1.13	1.07	1.13	1.07	1.14	1.15	1.19
	Trace elements (in ppm)						
La	6.3	7.3	7.3	6.20	14.07	7.79	3.89
Ce	18.5	18.2	21.1	15.1	31.3	22.4	9.5
Pr	2.63	3.00	4.33	2.09	3.49	3.19	1.61
Nd	11.3	14.3	23.4	9.8	12.7	15.2	8.3
Sm	6.89	8.78	14.3	4.38	3.21	8.40	5.76
Eu	0.01	0.02	0.02	0.04	0.55	0.01	0.06
Gd	11.8	14.9	19.3	6.50	2.99	12.8	9.9
Tb	2.68	3.30	4.15	1.29	0.50	3.52	2.74
Dy	22.4	27.6	31.0	10.5	3.1	26.5	20.8
Ho	4.62	5.86	5.38	2.53	0.61	6.50	5.05
Er	16.7	21.0	18.5	8.57	1.68	21.7	16.1
Tm	2.93	3.73	3.24	1.57	0.26	3.92	2.72
Yb	21.5	27.3	23.5	11.4	1.68	29.1	18.8
Lu	3.17	4.58	3.43	2.01	0.31	4.60	2.82
Y	178	215	122	104	19	333	190
Total REE	310	375	301	186	95	498	298
δEu	0.00	0.01	0.00	0.02	0.54	0.003	0.024
(La/Yb)N	0.20	0.18	0.21	0.37	6	0.18	0.14
Co	<0.2	0.30	0.30			0.67	0.04
Ni	5.90	2.90	4.80			0.26	<1
V	<8	<8	<8			0.72	<1
Th	23.4	22.9	11.7	17.3	10.3	29.3	38.4
Rb	510	485	515	529	220	618	523
Sr	1.90	2.20	1.9	5.73	75.4	1.46	13.8
Ba	<1	<1	3	17.4	274	<1	<1
Cs	37.0	45.2	10.8	31.2	20.3	34	12
Ta	4.90	5.80	7.00	6.95	1.78	5.72	3.41
Nb	15.5	15.4	15.4	15.0	8.40	21.4	17.7
Hf	5.70	9.90	4.90	4.45	2.30	6.63	8.24
Zr	63.8	76.9	29.0	50.9	70.5	72.9	86.6
Ga	33.6	32.9	38.5	29.9	14.4	39.3	53.4
Sc	2.0	2.0	4.0				
U	1.40	2.40	2.50	1.71	2.60	1.92	3.73

TABLE 2
(continued)

Pluton Name	**Jiangjunshan**		
Sample No.	**A5047**	**A5049**	**A5051**
Rock type	Differentiated granite	Differentiated granite	Differentiated granite
	Major elements (in wt %)		
SiO_2	76.28	70.02	74.83
TiO_2	0.01	0.02	0.01
Al_2O_3	13.08	16.05	14.42
Fe_2O_3	0.14	1.29	0.32
FeO	0.34	0.20	0.31
MnO	0.03	0.08	0.03
MgO	-0.12	-0.11	0.15
CaO	0.64	0.73	0.09
Na_2O	3.86	3.77	4.80
K_2O	3.87	5.75	4.59
P_2O_5	0.00	0.00	0.02
H_2O^+			
LOI	0.50	0.80	0.42
Total	98.62	98.59	99.99
A/NCK	1.12	1.17	1.11
	Trace elements (in ppm)		
La	6.41	11.94	9.23
Ce	16.2	34.2	25.8
Pr	2.71	5.78	3.75
Nd	13.6	28.8	16.8
Sm	8.23	18.5	8.05
Eu	0.02	0.02	0.53
Gd	13.2	28.0	8.8
Tb	3.52	7.84	2.41
Dy	26.0	58.9	16.9
Ho	6.25	14.0	3.72
Er	19.9	45.2	12.3
Tm	3.39	8.10	2.36
Yb	23.8	59.0	18.5
Lu	3.65	9.00	2.80
Y	276	435	84
Total REE	422	764	216
δEu	0.006	0.003	0.191
(La/Yb)N	0.18	0.14	0.34
Co	0.03	0.02	21.5
Ni	<1	0.14	38.2
V	9.77	6.97	172
Th	29.5	75.2	8.8
Rb	441	768	457
Sr	1.08	0.46	394
Ba	<1	<1	40.0
Cs	20	62	14
Ta	4.57	8.43	5.20
Nb	28.5	55.2	11.3
Hf	5.28	16.9	4.83
Zr	53.4	190	32.8
Ga	33.5	45.7	42.0
Sc			
U	3.97	3.66	2.13

Sample XSK-2 from Zhao and others, 1993.

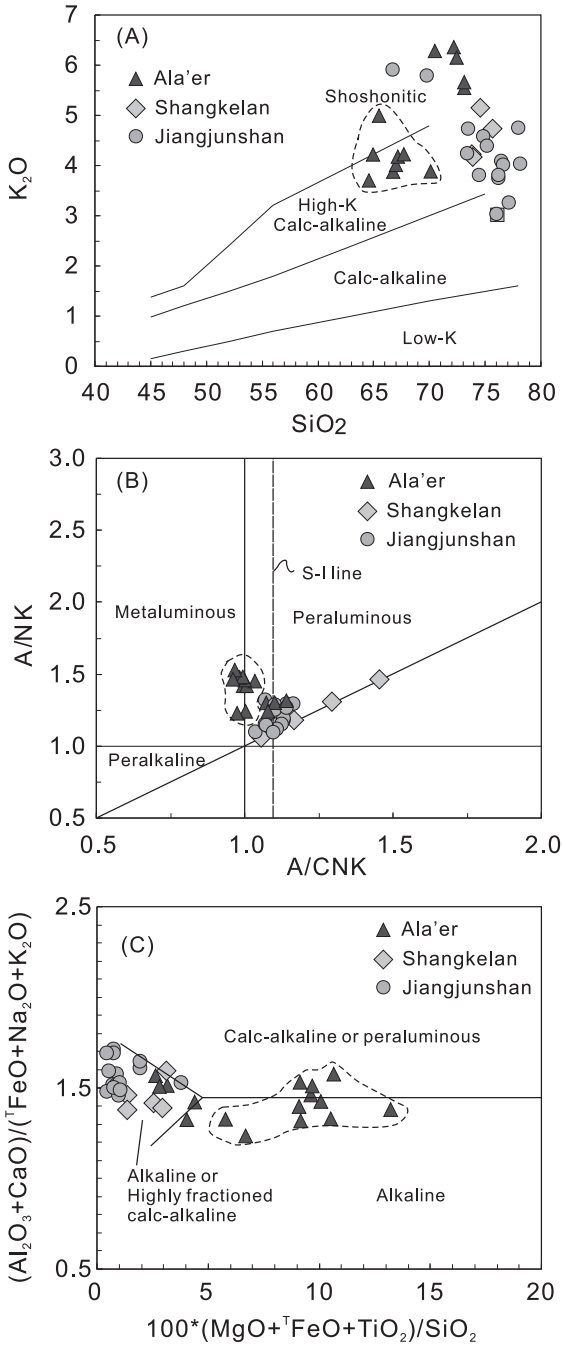

Fig. 5. Major element diagrams for the Mesozoic granites in the Chinese Altai. (A) K_2O vs. SiO_2 diagram (after Peccerillo and Taylor, 1976); (B) A/NK vs. A/CNK diagram (Shand's molar parameters in the diagram after Maniar and Piccoli, 1989), A/CNK = mol $Al_2O_3/(Na_2O + K_2O + CaO)$, A/NK = molar $Al_2O_3/(Na_2O + K_2O)$; (c) $((Al_2O_3 + CaO)/(FeO^* + Na_2O + K_2O))$ vs. 100 $(MgO + FeO^* + CaO)/SiO_2$ (after Sylvester, 1989). Same symbols as in figure 4. Data are from table 2. Additional major element data enveloped by a broken line for the Ala'er batholith are from Liu and others (1997).

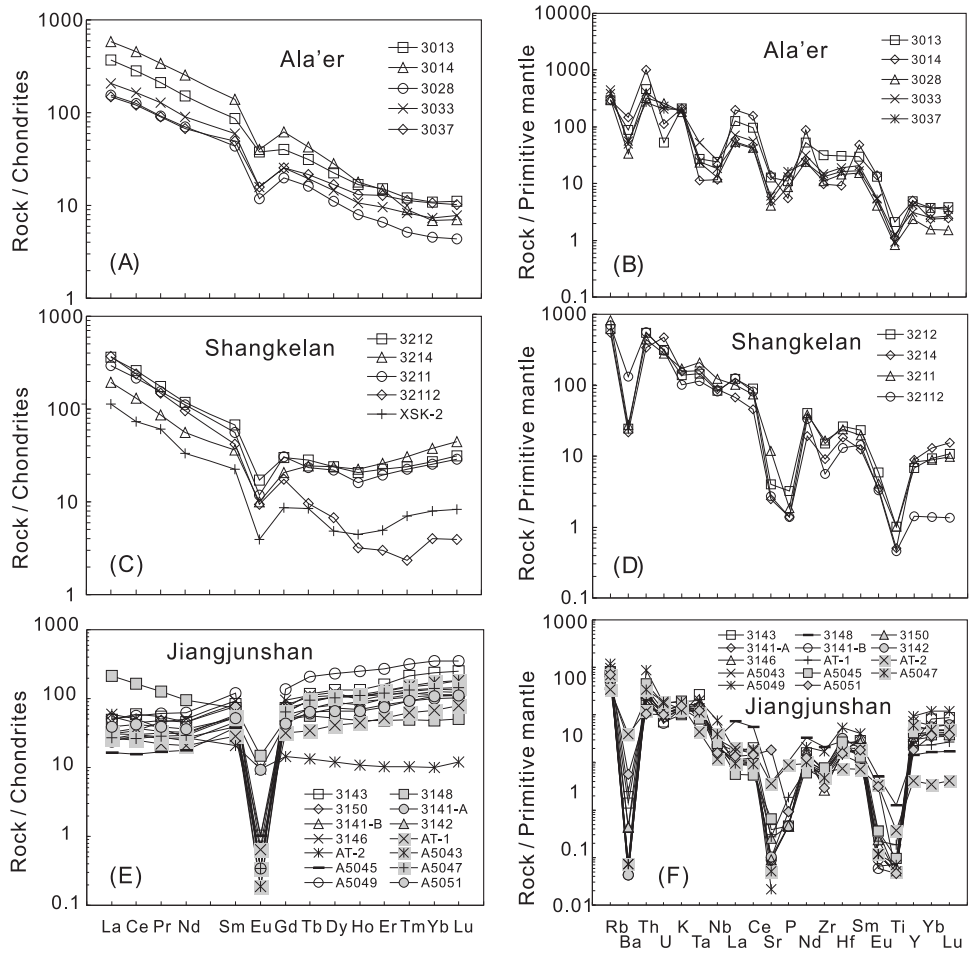

Fig. 6. REE patterns and spidergrams of the Mesozoic Ala'er (A and B), Shangkelan (C and D) and Jiangjunshan (E and F) granites from the Chinese Altai. The values of chondrite and primitive mantle are from Sun and McDonough (1989).

granitoids with $f_{Sm/Nd}$ values from −0.3 to −0.6 (falling between −0.2 and −0.6; table 3) give meaningful one-stage model ages (T_{DM1}) from 1.5 to 0.9 Ga. Some Jiangjunshan granites that have $f_{Sm/Nd}$ values from +0.38 to +0.97 give two-stage model ages (T_{DM1}) of 0.52 to 0.68 Ga (table 3).

Zircon Lu–Hf Isotopes

In situ zircon Hf isotopic analyses for 6 samples from the Mesozoic granitoids are presented in table 4. All analyses were carried out on magmatic zircon grains or domains with oscillatory zoning. Twenty eight Hf isotopic analyses for sample #3037 (monzogranite) from the Ala'er batholith (~210 Ma) have $\varepsilon_{Hf}(t)$ values of −1.9 to +4.0 (fig. 7B) and two-stage Hf model ages of 0.99 to 1.37 Ga. Eleven magmatic zircons from sample #3033 from the Ala'er batholith have $\varepsilon_{Hf}(216)$ values of −4.2 to +4.3 and two-stage Hf model ages of 0.98 to 1.52 Ga. Fifteen magmatic zircons from sample #3038, also from the Ala'er batholith, yield $\varepsilon_{Hf}(213)$ values ranging from −1.0 to +5 (fig. 7B) and two-stage Hf model ages from 0.94 to 1.33 Ga.

TABLE 3

Sr-Nd compositions for the Mesozoic granites from the Chinese Altai

Sample. No	Rock type	Pluton name	Age Ma	Rb ppm	Sr ppm	$^{87}Rb/^{86}Sr$	$^{87}Sr/^{86}Sr$	I_{Sr}	Sm ppm	Nd ppm	$^{147}Sm/^{144}Nd$	$^{143}Nd/^{144}Nd$	$\varepsilon_{Nd}(0)$	$f_{Sm/Nd}$	$\varepsilon_{Nd}(t)$	T_{DM-1} Ga	T_{DM-2} Ga	Mp %	Data source
3013	Porphyritic foliated granite	Ala'er	210	219	277.3	2.3	0.713304	0.7065	10.3	60.60	0.1025	0.512464	-3.4	-0.48	-0.9	0.94	1.06	56	This study
3028	Biotite monzogranite	Ala'er	210	223	82.6	7.8	0.734967	0.7116	5.75	29.10	0.1194	0.512331	-6.0	-0.39	-3.9	1.32	1.31	23	This study
3037	Porphyritic biotite monzogranite	Ala'er	210	277	117.9	6.8	0.730873	0.7105	6.08	27.61	0.1331	0.512368	-5.3	-0.32	-3.6	1.48	1.28	28	This study
	Porphyritic biotite monzogranite	Ala'er	210	16.1	268.5	0.2	0.713351	0.7128	8.56	49.44	0.1046	0.512387	-4.9	-0.47	-2.4	1.07	1.19	42	Wang and others, 2002
3214	Biotite granodiorite	Shangkelan	210	415	47.7	25	0.770097	0.6974	5.08	26.09	0.1177	0.512500	-2.7	-0.40	-0.6	1.03	1.03	58	This study
	Two mica granite	No. 60 granite	202	295	99.4	8.6	0.73766	0.7129	4.31	22.0	0.1183	0.512312	-6.4	-0.40	-4.3	1.34	1.33	17	Zhao and others, 1993
3150	Biotite granodiorite	Jiangjunshan	151	317	2.6	415.8	2.330682	1.4442	10.6	20.38	0.3142	0.512916	5.4	0.60	3.2	-0.36	0.69	83	This study
A-5043	Granite (main body)	Jiangjunshan	151						8.40	15.15	0.3352	0.512992	6.9	0.70	4.2	-0.20	0.60	89	This study
A-5045	Differentiated granite	Jiangjunshan	151						5.76	8.25	0.4221	0.513127	9.5	1.15	5.2	-0.02	0.52	93	This study
A-5047	Differentiated granite	Jiangjunshan	151						8.23	13.64	0.3648	0.513039	7.8	0.85	4.6	-0.11	0.57	90	This study
A-5049	Differentiated granite	Jiangjunshan	151						18.46	28.84	0.3870	0.513073	8.5	0.97	4.8	-0.07	0.55	91	This study
A-5051	Amazonite granite	Jiangjunshan	151						8.05	16.76	0.2904	0.512997	7.0	0.48	5.2	-0.31	0.52	93	This study
AT-1	Two mica monzogranite	Jiangjunshan	151	510	6.2	259.5	1.652280	1.0990	4.31	10.11	0.2576	0.512922	5.5	0.31	4.4	-0.80	0.59	89	Chen and Jahn, 2002
AT-1*	Two mica monzogranite	Jiangjunshan	151	509	6.2	261.2	1.658548	1.1016	3.99	8.91	0.2711	0.512930	5.7	0.38	4.3	-0.59	0.60	89	Chen and Jahn, 2002
	Amazonite granite	Jiangjunshan	151						9.67	42.88	0.1362	0.512648	0.2	-0.31	1.4	0.99	0.83	73	Zhao and others, 1993
	Amazonite granite	Jiangjunshan	151						9.98	44.23	0.1363	0.512632	-0.1	-0.31	1.0	1.02	0.85	71	Zhao and others, 1993

Note: $\varepsilon_{Nd} = ((^{143}Nd/^{144}Nd)_s/(^{143}Nd/^{144}Nd)_{CHUR} - 1)*10000$, $f_{Sm/Nd} = (^{147}Sm/^{144}Nd)_s/(^{147}Sm/^{144}Nd)_{CHUR} - 1$, where s = sample, $(^{143}Nd/^{144}Nd)_{CHUR} = 0.512638$, and $(^{147}Sm/^{144}Nd)_{CHUR} = 0.1967$. The one-stage model ages ($T_{DM}-1$) were calculated using a linear isotopic ratio growth equation: $T_{DM-1} = 1/\lambda x \ln(1 + ((^{143}Nd/^{144}Nd)_s - 0.51315)/((^{147}Sm/^{144}Nd)_s - 0.2137))$. $T_{DM-2} = ((10 - \varepsilon_{Nd}(0) + 25.1*\text{Age (in Ga)}*(f_{Sm/Nd} + 0.4)))/(25.1*(0.086+0.4))$. T_{DM} is used model age. Mp is the proportion of mantle-derived component estimated by $Mp = Ndc \times (\varepsilon c - \varepsilon r)/[\varepsilon r \times (Ndm - Ndc) - (\varepsilon m \times Ndm - \varepsilon c \times Ndc)] \times 100$ (Jahn and others, 2004), where Mp = % mantle-derived juvenile component; εc, εr, εm = Nd isotopic compositions of the crust, rock measured, and mantle component, respectively. Ndc, Ndm = Nd concentrations in the crust and mantle components, respectively. See the text.

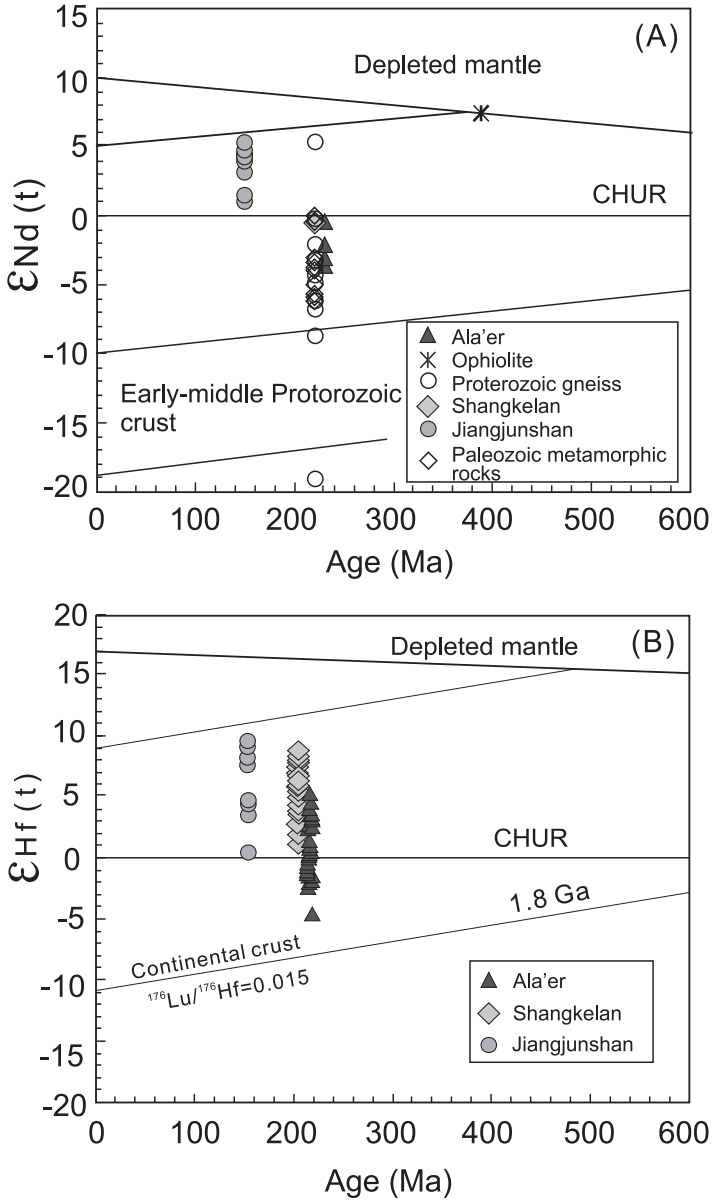

Fig. 7. (A) $\varepsilon_{Nd}(t)$ and (B) $\varepsilon_{Hf}(t)$ vs. Intrusive age diagrams. T_{DM2} for samples with Sm/Nd >0.15 (or ($f_{Sm/Nd} > -0.2$ and < -0.6). Data for the Proterozoic gneiss, Paleozoic metamorphic rocks and ophiolite are from Hu and others (2000), Chen and Jahn (2002) and Xu and others (2003), respectively. The $\varepsilon_{Nd}(t)$ values of the Proterozoic gneisses have been recalculated using 220 Ma to evaluate if they can be the sources for the granites (220 Ma).

Thirty-eight Hf isotopic analyses for sample #3214 (granodiorite) from the Shangkelan pluton (~202 Ma, zircon age) show positive $\varepsilon_{Hf}(t)$ values of +1.2 to +7.7 and slightly younger Hf model ages of 0.75 to 1.17 Ga when compared to the Ala'er batholith samples. Seven magmatic zircons from sample #3141A of the Jiangjunshan pluton have positive $\varepsilon_{Hf}(151)$ values of +0.5 to +8.8 (fig. 7B) and two-stage Hf model

TABLE 4

Zircon in-situ Hf isotopic analyses for the Mesozoic granites from the Chinese Altai

Sample No.	t (Ma)	$^{176}Yb/^{177}Hf$	$^{176}Lu/^{177}Hf$	$^{176}Hf/^{177}Hf$	$2\sigma_m$	$\varepsilon_{Hf}(0)$	$\varepsilon_{Hf}(t)$	2σ	$f_{Lu/Hf}$	T_{DM1}(Hf) (Ga)	T_{DM2}(Hf) (Ga)
3037 Monzogranite, Ala'er pluton											
1	210	0.089603	0.002117	0.282746	24	-0.9	3.4	0.9	-0.936	0.74	1.03
2	210	0.100157	0.002368	0.282704	21	-2.4	1.9	0.8	-0.929	0.81	1.13
3	210	0.069283	0.001597	0.282691	19	-2.9	1.5	0.7	-0.952	0.81	1.15
4	210	0.043407	0.000899	0.282744	23	-1.0	3.5	0.8	-0.973	0.72	1.03
5	210	0.094039	0.002102	0.282732	18	-1.4	2.9	0.6	-0.937	0.76	1.06
6	210	0.060373	0.001408	0.282733	23	-1.4	3.0	0.8	-0.958	0.74	1.05
7	210	0.053628	0.001238	0.282683	18	-3.1	1.3	0.6	-0.963	0.81	1.17
8	210	0.082933	0.001981	0.282708	27	-2.3	2.1	0.9	-0.94	0.79	1.12
9	210	0.092173	0.002137	0.282744	23	-1.0	3.3	0.8	-0.936	0.74	1.04
10	210	0.064706	0.001482	0.282711	23	-2.2	2.2	0.8	-0.955	0.78	1.11
11	210	0.056367	0.001356	0.282632	20	-5.0	-0.5	0.7	-0.959	0.89	1.28
12	210	0.098915	0.002257	0.282697	22	-2.6	1.7	0.8	-0.932	0.81	1.14
13	210	0.032020	0.000775	0.282645	23	-4.5	0.0	0.8	-0.977	0.86	1.25
14	210	0.039886	0.000898	0.282681	24	-3.2	1.3	0.8	-0.973	0.81	1.17
15	210	0.110059	0.002554	0.282651	38	-4.3	0.0	1.3	-0.92	0.89	1.25
16	210	0.068153	0.001564	0.282696	27	-2.7	1.7	1.0	-0.95	0.80	1.14
17	210	0.077854	0.001902	0.282763	21	-0.3	4.0	0.7	-0.94	0.71	0.99
18	210	0.082061	0.001919	0.282595	26	-6.3	-1.9	0.9	-0.94	0.95	1.37
19	210	0.104104	0.002339	0.282733	24	-1.4	2.9	0.8	-0.93	0.76	1.06
20	210	0.083754	0.001704	0.282677	30	-3.4	1.0	1.1	-0.95	0.83	1.18
21	210	0.108893	0.002054	0.282723	28	-1.7	2.6	1.0	-0.94	0.77	1.08
22	210	0.082717	0.001738	0.282630	33	-5.0	-0.7	1.2	-0.95	0.90	1.29
23	210	0.075604	0.001615	0.282722	24	-1.8	2.6	0.9	-0.95	0.76	1.08
24	210	0.089649	0.001899	0.282697	23	-2.7	1.7	0.8	-0.94	0.81	1.14
25	210	0.090256	0.001955	0.282642	27	-4.6	-0.3	1.0	-0.94	0.89	1.27
26	210	0.081020	0.001584	0.282683	32	-3.1	1.3	1.1	-0.95	0.82	1.17
27	210	0.155400	0.003066	0.282767	35	-0.2	4.0	1.2	-0.91	0.73	0.99
28	210	0.047389	0.000926	0.282618	23	-5.4	-1.0	0.8	-0.97	0.90	1.31
3033 Monzogranite, Ala'er pluton											
1	216	0.106923	0.002406	0.282529	41	-8.6	-4.2	1.5	-0.93	1.06	1.52
2	216	0.129865	0.003192	0.282614	36	-5.6	-1.3	1.3	-0.9	0.96	1.34
3	216	0.235508	0.005378	0.282603	57	-6.0	-1.9	2.0	-0.84	1.04	1.38
4	216	0.103514	0.002260	0.282744	39	-1.0	3.4	1.4	-0.93	0.75	1.04
5	216	0.131090	0.003184	0.282672	35	-3.5	0.7	1.2	-0.9	0.87	1.21
6	216	0.130352	0.002977	0.282735	41	-1.3	3.0	1.4	-0.91	0.77	1.06
7	216	0.130992	0.002500	0.282738	31	-1.2	3.2	1.1	-0.92	0.76	1.05
8	216	0.104727	0.002246	0.282619	43	-5.4	-0.9	1.5	-0.93	0.93	1.31
9	216	0.157413	0.003350	0.282773	26	0.0	4.3	0.9	-0.9	0.73	0.98
10	216	0.137977	0.003363	0.282724	34	-1.7	2.6	1.2	-0.9	0.80	1.09
11	216	0.056390	0.001302	0.282616	22	-5.5	-1.0	0.8	-0.96	0.91	1.31
3038 Monzogranite, Ala'er pluton											
1	213	0.075184	0.001302	0.282738	19	-1.2	3.3	0.7	-0.96	0.73	1.04
2	213	0.093251	0.001736	0.282655	17	-4.1	0.3	0.6	-0.95	0.86	1.23
3	213	0.214287	0.003099	0.282765	23	-0.2	4.0	0.8	-0.91	0.73	1.00
4	213	0.189961	0.003448	0.282625	21	-5.2	-1.0	0.8	-0.9	0.95	1.32
5	213	0.093114	0.001491	0.282716	22	-2.0	2.5	0.8	-0.96	0.77	1.09
6	213	0.135532	0.003007	0.282665	15	-3.8	0.5	0.5	-0.91	0.88	1.22
7	213	0.083250	0.001464	0.282684	21	-3.1	1.3	0.7	-0.96	0.82	1.17
8	213	0.073315	0.001260	0.282660	18	-3.9	0.6	0.6	-0.96	0.84	1.22
9	213	0.093396	0.001713	0.282784	20	0.4	4.9	0.7	-0.95	0.68	0.94

Table 4
(continued)

Sample No.	t (Ma)	$^{176}Yb/^{177}Hf$	$^{176}Lu/^{177}Hf$	$^{176}Hf/^{177}Hf$	$2\sigma_m$	$\varepsilon_{Hf}(0)$	$\varepsilon_{Hf}(t)$	2σ	$f_{Lu/Hf}$	T_{DM1}(Hf) (Ga)	T_{DM2}(Hf) (Ga)
3038 Monzogranite, Ala'er pluton											
10	213	0.091260	0.001714	0.282691	17	-2.9	1.5	0.6	-0.95	0.81	1.15
11	213	0.167144	0.004164	0.282686	26	-3.0	1.1	0.9	-0.87	0.88	1.18
12	213	0.137631	0.002549	0.282728	20	-1.5	2.7	0.7	-0.92	0.77	1.08
13	213	0.146323	0.003813	0.282692	24	-2.8	1.3	0.9	-0.89	0.86	1.17
14	213	0.095563	0.001850	0.282690	19	-2.9	1.5	0.7	-0.94	0.82	1.16
15	213	0.118369	0.002842	0.282613	24	-5.6	-1.4	0.8	-0.91	0.95	1.34
3214 Granodiorite, Shangkelan pluton											
1	202	0.118180	0.003315	0.282790	16	0.6	4.6	0.6	-0.90	0.70	0.95
2	202	0.248197	0.006457	0.282792	31	0.7	4.3	1.1	-0.81	0.76	0.97
3	202	0.109341	0.003000	0.282821	15	1.7	5.8	0.5	-0.91	0.65	0.87
4	202	0.091085	0.002188	0.282807	13	1.2	5.4	0.5	-0.93	0.65	0.90
5	202	0.105944	0.003049	0.282792	16	0.7	4.7	0.6	-0.91	0.69	0.94
6	202	0.151409	0.003493	0.282825	21	1.9	5.8	0.7	-0.89	0.65	0.87
7	202	0.074599	0.001874	0.282799	19	1.0	5.1	0.7	-0.94	0.66	0.91
8	202	0.065882	0.001601	0.282793	17	0.7	4.9	0.6	-0.95	0.66	0.93
9	202	0.055155	0.001377	0.282772	22	0.0	4.2	0.8	-0.96	0.69	0.97
10	202	0.122112	0.003168	0.282854	16	2.9	6.9	0.6	-0.90	0.60	0.80
11	202	0.104016	0.002610	0.282821	17	1.7	5.8	0.6	-0.92	0.64	0.87
12	202	0.059554	0.001647	0.282750	26	-0.8	3.4	0.9	-0.95	0.72	1.02
13	202	0.065018	0.001657	0.282712	19	-2.1	2.1	0.7	-0.95	0.78	1.11
14	202	0.088305	0.002473	0.282787	37	0.5	4.6	1.3	-0.93	0.69	0.95
15	202	0.054980	0.001284	0.282732	20	-1.4	2.9	0.7	-0.96	0.74	1.06
16	202	0.124828	0.003200	0.282734	40	-1.3	2.7	1.4	-0.90	0.78	1.07
17	202	0.051002	0.001201	0.282818	14	1.6	5.9	0.5	-0.96	0.62	0.87
18	202	0.089777	0.002394	0.282800	26	1.0	5.1	0.9	-0.93	0.67	0.92
19	202	0.118126	0.002898	0.282779	16	0.3	4.3	0.6	-0.91	0.71	0.97
20	202	0.061508	0.001575	0.282810	20	1.4	5.6	0.7	-0.95	0.64	0.89
21	202	0.099389	0.002547	0.282859	13	3.1	7.2	0.5	-0.92	0.58	0.78
22	202	0.057595	0.001352	0.282865	14	3.3	7.5	0.5	-0.96	0.55	0.76
23	202	0.115366	0.003058	0.282889	9	4.1	8.2	0.3	-0.91	0.55	0.72
24	202	0.047883	0.001288	0.282868	21	3.4	7.7	0.7	-0.96	0.55	0.75
25	202	0.094754	0.002116	0.282835	22	2.2	6.4	0.8	-0.94	0.61	0.84
26	202	0.030557	0.000656	0.282767	20	-0.2	4.2	0.7	-0.98	0.68	0.98
27	202	0.106667	0.002521	0.282791	19	0.7	4.8	0.7	-0.92	0.68	0.94
28	202	0.033781	0.000882	0.282759	20	-0.5	3.9	0.7	-0.97	0.70	1.00
29	202	0.126731	0.002549	0.282858	25	3.0	7.1	0.9	-0.92	0.58	0.79
30	202	0.043646	0.000941	0.282768	20	-0.1	4.2	0.7	-0.97	0.68	0.98
31	202	0.097930	0.002510	0.282788	17	0.6	4.7	0.6	-0.92	0.69	0.95
32	202	0.096997	0.002085	0.282874	23	3.6	7.8	0.8	-0.94	0.55	0.75
33	202	0.085133	0.001843	0.282813	19	1.5	5.6	0.7	-0.94	0.64	0.88
34	202	0.083753	0.001931	0.282760	16	-0.4	3.7	0.6	-0.94	0.72	1.00
35	202	0.049805	0.001387	0.282859	30	3.1	7.3	1.1	-0.96	0.56	0.78
36	202	0.091505	0.002599	0.282691	28	-2.9	1.2	1.0	-0.92	0.83	1.17
37	202	0.145879	0.003031	0.282760	23	-0.4	3.6	0.8	-0.91	0.74	1.01
38	202	0.058273	0.001849	0.282835	24	2.2	6.4	0.8	-0.94	0.60	0.83

TABLE 4

(continued)

Sample No.	t (Ma)	$^{176}Yb/^{177}Hf$	$^{176}Lu/^{177}Hf$	$^{176}Hf/^{177}Hf$	$2\sigma_m$	$\varepsilon_{Hf}(0)$	$\varepsilon_{Hf}(t)$	2σ	$f_{Lu/Hf}$	$T_{DM1}(Hf)$ (Ga)	$T_{DM2}(Hf)$ (Ga)
3141A Monzogranite, Jiangjunshan pluton											
10	213	0.091260	0.001714	0.282691	17	-2.9	1.5	0.6	-0.95	0.81	1.15
1	151	0.217007	0.003978	0.282811	37	1.4	4.3	1.3	-0.88	0.68	0.93
2	151	0.363906	0.006898	0.282946	69	6.1	8.8	2.4	-0.79	0.52	0.64
3	151	0.271000	0.006028	0.282783	65	0.4	3.1	2.3	-0.82	0.77	1.01
4	151	0.398280	0.006795	0.282896	46	4.4	7.0	1.6	-0.8	0.60	0.76
5	151	0.184618	0.003062	0.282800	43	1.0	4.0	1.5	-0.91	0.68	0.95
6	151	0.181055	0.003059	0.282891	48	4.2	7.2	1.7	-0.91	0.54	0.74
7	151	0.252182	0.004132	0.282705	49	-2.4	0.5	1.8	-0.88	0.85	1.17
3150 Monzogranite, Jiangjunshan pluton											
1	151	0.467791	0.010577	0.282900	201	4.5	6.8	7.1	-0.68	0.67	0.77
2	151	0.190279	0.004101	0.282922	19	5.3	8.2	0.7	-0.88	0.51	0.68
3	151	0.220976	0.004972	0.282899	22	4.5	7.3	0.8	-0.85	0.56	0.74

Note: $\varepsilon_{Hf}(0) = ((^{176}Hf/^{177}Hf)/(^{176}Hf/^{177}Hf)_{CHUR,0} - 1) \times 10000$, $f_{Lu/Hf} = (^{176}Lu/^{177}Hf)/(^{176}Lu/^{177}Hf)_{CHUR} - 1$.

$\varepsilon_{Hf}(t) = ((^{176}Hf/^{177}Hf)_s - (^{176}Lu/^{177}Hf)_s \times (e^{\lambda t} - 1))/((^{176}Hf/^{177}Hf)_{CHUR,0} - (^{176}Lu/^{177}Hf)_{CHUR} \times (e^{\lambda t} - 1)) - 1) \times 10{,}000$.

$T_{DM1}(Hf) = 1/\lambda \times (1 + ((^{176}Hf/^{177}Hf)_s - (^{176}Hf/^{177}Hf)_{DM})/((^{176}Lu/^{177}Hf)_s - (^{176}Lu/^{177}Hf)_{DM}))$.

$T_{DM2}(Hf) = T_{DM1}(Hf) - (T_{DM1}(Hf) - t)((f_{CC} - f_S)/(f_{CC} - f_{DM}))$; where $(^{176}Lu/^{177}Hf)_s$ and $(^{176}Hf/^{177}Hf)_s$ are the measured values of samples; $(^{176}Lu/^{177}Hf)_{CHUR} = 0.0332$ and $(^{176}Hf/^{177}Hf)_{CHUR,0} = 0.282772$; $(^{176}Lu/^{177}Hf)_{DM} = 0.0384$ and $(^{176}Hf/^{177}Hf)_{DM} = 0.28325$; $f_{CC} = -0.548$ (average continental crust), $f_{DM} = 0.16$, t = crystallization time of zircon, $\lambda = 1.865 \times 10^{-11}$ yr^{-1} reported by Scherer and others (2001) is used in the calculation.

ages of 0.64 Ga to 1.17 Ga. The three zircons from sample #3150 (biotite granite) from the Jiangjunshan pluton (~150 Ma) also have positive $\varepsilon_{Hf}(t)$ values of +6.8 to +8.2 (fig. 7B) and young two-stage Hf model ages of 0.68 to 0.77 Ga (table 4).

DISCUSSION

Timing and Distribution of Mesozoic Magmatism in the Altai

The U-Pb zircon dating of the Ala'er and Shangkelan samples using three different techniques (TIMS, LA-ICPMS and SHRIMP) yield similar ages of 212 ± 2, 216 ± 1, 211 ± 3, 213 ± 1 Ma, and 203 ± 3 Ma, indicating the coeval nature of the intrusions. This is the first identification of early Mesozoic (Triassic) magmatism from the Chinese Altai by zircon dating. In addition, we had previously obtained four U-Pb SHRIMP zircon ages (220 to 198 Ma) from the "No. 3 granitic pegmatite" in Unit 3 of the eastern Chinese Altai (Wang and others, 2007; fig. 1). This pegmatite hosts the most important mine for Li mineralization in Asia and is one of the largest pegmatites in the world. Previously, several Ar-Ar dates of 220 to 180 Ma have also been obtained from granitic and pegmatite intrusions and their mineralized deposits in the Chinese Altai (Chen and other, 2000; Wang and other, 2002). All the above age data indicate that an early Mesozoic (220-200 Ma) tectonothermal event is more significant than previously thought in the Chinese Altai.

On the other hand, the Jiangjunshan pluton is dated at 151 ± 3 Ma. So far, this is the only late Jurassic pluton identified from the Chinese Altai. Other Jurassic or even younger granitoids in the Altai orogen perhaps remain to be discovered.

Several K-Ar, Ar-Ar and Rb-Sr dates ranging from 270 to 130 Ma have also been reported for granites in the Chinese Altai. For example, 250 Ma (Rb-Sr; Liu, 1990) and

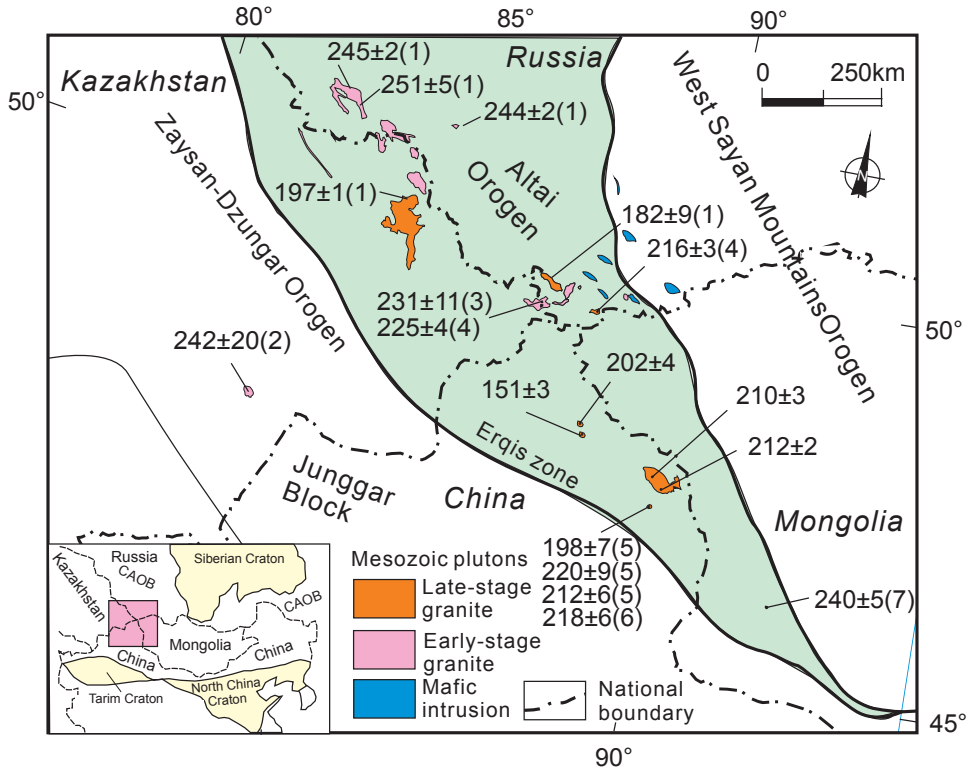

Fig. 8. Distribution of the Mesozoic intrusions in the Altai Mountains of four countries (Russia, Kazakhstan, Mongolia and China). The ages are all zircon ages. Ages sources: (1) Vladimirov and others, 2005; (2) Dokukina and others, 2010; (3) Vladimirov and others, 1997; (4) Annikova and others, 2006; (5) Wang and others, 2007; (6) Zhu and others, 2006; (7) Kozakov and others, 1997.

131 Ma (Ar-Ar; Zhang and others, 1994) ages have been reported from the Ala'er batholith; 176 ± 13 Ma (Rb-Sr; Zhang and others, 1994), 183 ± 38 Ma (Rb-Sr; Hu and others, 1997) and 183 ± 9 Ma (Rb-Sr; Chen and others, 2000) ages from the Shangkelan pluton; and 220 ± 0.3 Ma (Ar-Ar; Zhang and others, 1994), 235 Ma (Rb-Sr) and 207 Ma (K-Ar; cited from Zhang and others, 1994) from the Jiangjunshan pluton. The dates for the Shangkelan pluton are similar or younger than our zircon ages, and they could be interpreted as cooling ages or due to overprinting by a late thermal event. However, some Rb-Sr and Ar-Ar dates for the Ala'er and Jiangjunshan intrusions are markedly different from our zircon ages and their significance is unclear.

Early Mesozoic (Early Triassic-Early Jurassic) intrusions are also exposed sporadically in the Russian, Kazakhstan and Mongolian Altai (fig. 8; Vladimirov and others, 2001, 2005; Annikova and others, 2006; Pavlova and others, 2008). These intrusions have zircon ages ranging from 253 to 180 Ma (table 4). The Early-Middle Triassic (250-228 Ma) intrusions mainly occur in the Russian and Kazakhstan Altai, particularly in the western segment of the Mesozoic intrusive belt in the Altai. They include the 237 ± 4 Ma granite of the Artukol massif in the Russian Altai (Gusev, 2004) and the amphibole–biotite granite (242 ± 20 Ma) of the Tastau Complex in the Kazakhstan Altai (Dokukina and others, 2010). Coeval alkaline mafic dikes are also exposed in this magmatic belt (Pavlova and others, 2008). A small Early Triassic granitic intrusion

(240 ± 5 Ma) is exposed in the middle reach of the Uench River in the Mongolian Altai (Kozakov and others, 1997).

The Late Triassic–Early Jurassic (228-180 Ma) intrusions are mainly distributed in the Chinese Altai (fig. 8), and are represented by the granites (200-210 Ma) of the present study and the No. 3 pegmatites (220-198 Ma, SHRIMP zircon U-Pb ages; Zhu and others, 2006; Wang and others, 2007). Yuan and others (2011) also reported a Late Triassic hornblende Ar-Ar age for the Ashele basalt in the Altai area. Late Triassic granitoids also occur in the Russian Altai, for example, a granite from the Kalguta Mo-W ore-magmatic belt has a zircon age of 216 ± 3 Ma (Annikova and others, 2006), and a leucogranite from the Chigerteand Sagsai Massif has a zircon age of 225 ± 10 Ma (Demin and others, 2001). At present, only one Late Jurassic (amazonite-bearing) granitic pluton (the Jiangjunshan pluton) has been recognized in the Chinese Altai.

In summary, the Early Mesozoic intrusions in the Altai are mainly distributed in the central part of the Altai orogen, near the national boundaries between China, Russia and Kazakhstan (fig. 8). These intrusions were emplaced in several stages. The early-stage (Early-Middle Triassic, 250-228 Ma) intrusions mainly occur in the western and eastern Altai (the Russian Altai and Mongolian Altai), and the late-stage (Late Triassic-Early Jurassic, 228-180 Ma) in the central Altai (the Chinese-Russian Altai). The only Late Jurassic pluton (Jiangjunshan pluton, 151 ± 3 Ma) occurs in the southern Altai.

Origin of the Granites

The Late Triassic Ala'er granites in the Chinese Altai have high K_2O contents and show shoshonitic characteristics (fig. 5). In the spidergrams, the negative anomalies in Ba, P, Nb, Ta, Ti and particularly Sr, and pronounced positive anomalies in Rb, Th, K and La are indicative of involvement of crustal melts and advanced fractional crystallization (fig. 6). Liu and others (1997) suggested that the Ala'er granites are S-type based on the ACF triangular diagram (White and Chappell, 1988). However, their weak peraluminous or metaluminous-peraluminous characteristics (table 2) imply they are not typical S-types. The negative correlation between P_2O_5 and SiO_2 appears to follow the I-type trend (fig. 9), which was considered as an effective means for distinction of I- from S-type granites by Chappell and White (1992). Thus, the Ala'er granites are I-type, or more likely highly-evolved I-type granites. In the granite discrimination diagrams (fig. 10), the Ala'er granites plot in the A-type field.

The Late Triassic Shangkelan granites are high-K calc-alkaline (fig. 5A), peraluminous (fig. 5B), and highly differentiated (fig. 5C). Their trace element patterns also show the characteristics of advanced differentiation, characterized by strong Eu-depletion and distinct negative anomalies in Ba, Sr, P and Ti and positive anomalies in Rb and K (figs. 6C and 6D). In summary, the trace element data show features typical of A-type (fig. 10; Whalen and others, 1987) or highly differentiated I-type granites (figs. 5C and 6).

The Early Jurassic Jiangjunshan granites belong to the calc-alkaline to high-K calc-alkaline series (fig. 5A) and are peraluminous (fig. 5C). The REE patterns of most Jiangjunshan samples show the lanthanide tetrad effect (fig. 6E). In the spidergrams, all the samples show negative anomalies for Ba, Sr, P, Eu and Ti, and positive for Th and Nd (fig. 6F). These features, along with the presence of amazonite, indicate that they are typical A-type granites (fig. 10).

The REE tetrad effect is well known for highly differentiated felsic rocks with strong fluid-melt interaction in the late stage of differentiation (for example, Bau, 1996; Irber, 1999; Jahn and others, 2004), and has recently been documented for highly differentiated granites from NE China (Jahn and others, 2001; Wu and others, 2004), Mongolia (Jahn and others, 2004) and the Junggar Block (Chen and Jahn, 2004). The Jiangjunshan granites were therefore probably developed via a process

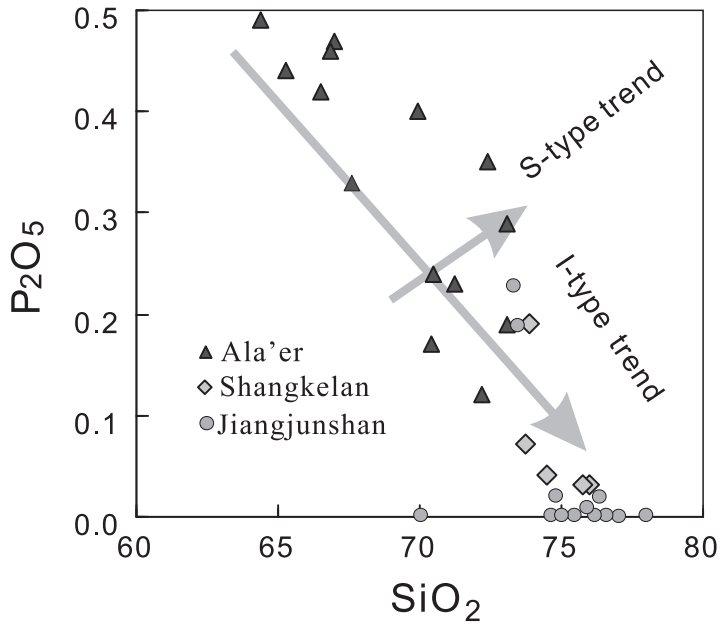

Fig. 9. P_2O_5 vs. SiO_2 diagram for the Mesozoic granitoids, showing I- and S-type granites and the variation of P_2O_5 as a function of SiO_2 content (Chappell and White, 1992).

involving strong fluid-melt interaction. These granites contain garnet and muscovite, and are weakly peraluminous.

In the Russian Altai, the early Mesozoic (Triassic) granites comprise not only the more common granodiorite-quartz diorite, biotite granite, two-mica monzogranite, and muscovite granite association, but also the less common syenite-granite and leucogranite with garnet, tourmaline and cordierite association. In addition, the granites are commonly associated with coeval alkaline mafic dikes and lavas (see Pavlova and others, 2008). These granites could be produced by differentiation of mantle-derived alkaline mafic liquids with the signature of mantle plumes and the granite-leucogranite might have been formed by an interaction between mafic and felsic magmas (Vladimirov and others, 2005; Annikova and others, 2006; Pavlova and others, 2008; Dokukina and others, 2010).

Nd-Hf Isotopic Constraints on the Nature of the Protoliths

We have previously undertaken Nd isotopic mapping of the intrusions in the Chinese Altai (Wang and others, 2009a; figs. 11A and 11B). As shown in figure 11A, intrusions with negative to weakly positive $\varepsilon_{Nd}(t)$ values of -4 to $+2$ occur in the central Altai (Units 2/3), whereas those with higher positive values of $+1.4 - +6$ occur in the southern Altai (Units 4/5). Granitoids from the Junggar terrane (Unit 6) have the highest $\varepsilon_{Nd}(t)$ values up to $+8.4$. Correspondingly, Nd model ages (T_{DM}) decrease from 1.6 to 1.1 Ga in the central Altai to 1.0 to 0.5 Ga in the southern Altai, except for a continental fragment in Unit 4 (fig. 11B). These results imply that the central Altai contains widespread old crustal components (*ca.* 1600-1000 Ma) in the granite source regions, whereas the southern Altai comprises a higher proportion of juvenile mantle-derived rocks.

The Ala'er and Shangkelan granitic plutons occur exclusively in the central Altai (old terrane), which is, the "Altai microcontinent" (or Unit 3). Consequently, the

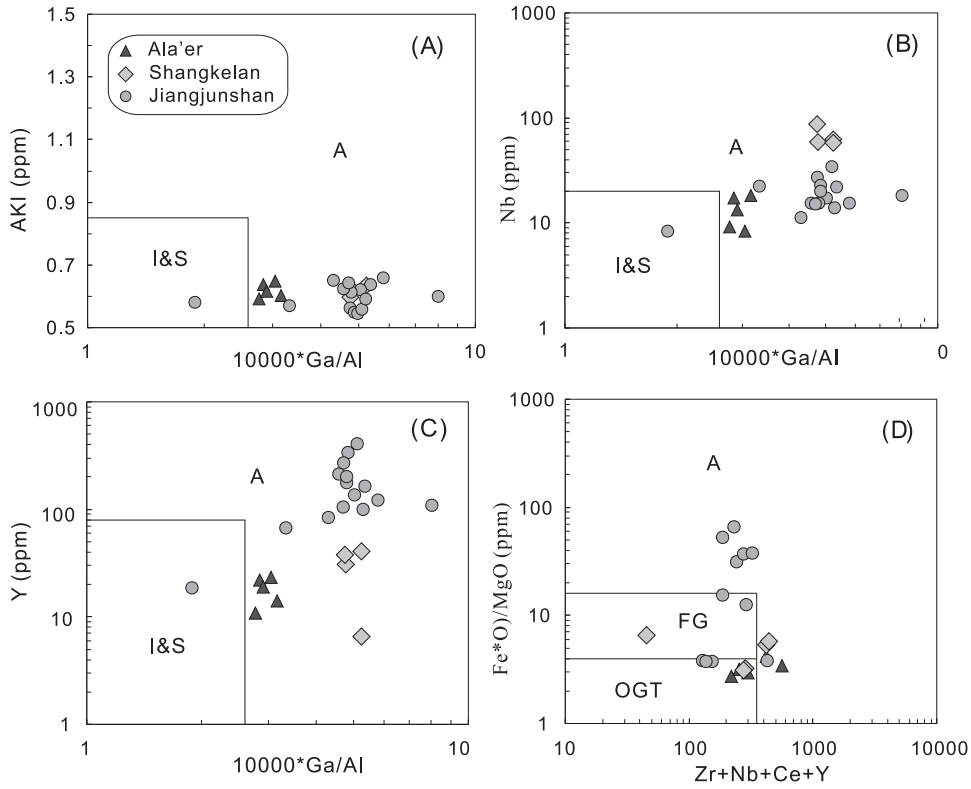

Fig. 10. Plots of the Mesozoic granitoids in discrimination diagrams for A-type granitoids. (A), (B), (C) AKI, Nb, and Y contents vs. 10,000*Ga/A, respectively, correlation diagrams; (D) FeO*/MgO vs. (Zr +Nb + Ce +Y) correlation diagram (Whalen and others, 1987). I, S and A = I-, S- and A-type granitoids; FG = Fractionated felsic granites; OGT = Orogenic I-/S-type granitoids.

suspected Proterozoic basement rocks are expected to have made a significant contribution to the generation of the granites. Indeed, these granites have negative whole-rock $\varepsilon_{Nd}(t)$ values (−4.2 to −0.6) and Proterozoic model ages (1.5-0.9 Ga). On the other hand, the zircon Hf isotopic data provide somewhat different information. The granites from the Ala'er and Shangkelan plutons show $\varepsilon_{Hf}(t)$ values slightly higher than $\varepsilon_{Nd}(t)$ values, implying a possible Nd-Hf isotope decoupling (fig. 7). One interpretation is that these granites were derived from an old crustal source with involvement of depleted mantle-derived materials with high $\varepsilon_{Hf}(t)$ values (for example, Yang and others, 2007), or that there was insufficient mixing between the two components during the melting process, or perhaps heterogeneous contamination (Zheng and others, 2007). Whatever the case, the variable high zircon $\varepsilon_{Hf}(t)$ values (−4.0 to +8.2) indicate that a juvenile mantle-derived component played a more important role than basement rocks in the generation of the granitic rocks (fig. 7).

The Jiangjunshan pluton occurs at the northern margin of the southern Altai (young accretionary terrane, Unit 4), thus, in comparison with the Ala'er and Shangkelan intrusions, it has higher positive whole-rock $\varepsilon_{Nd}(t)$ values (+1.0 to +5.2) and younger model ages (T_{DM} = 0.36-1.02 Ga), as well as strong positive zircon $\varepsilon_{Hf}(t)$ values (+0.5 to +8.9) and young Hf model ages (0.64 Ga-1.17 Ga). Since the $\varepsilon_{Nd}(t)$ values are higher than those of the felsic gneisses and schists in the region (fig. 7A), the

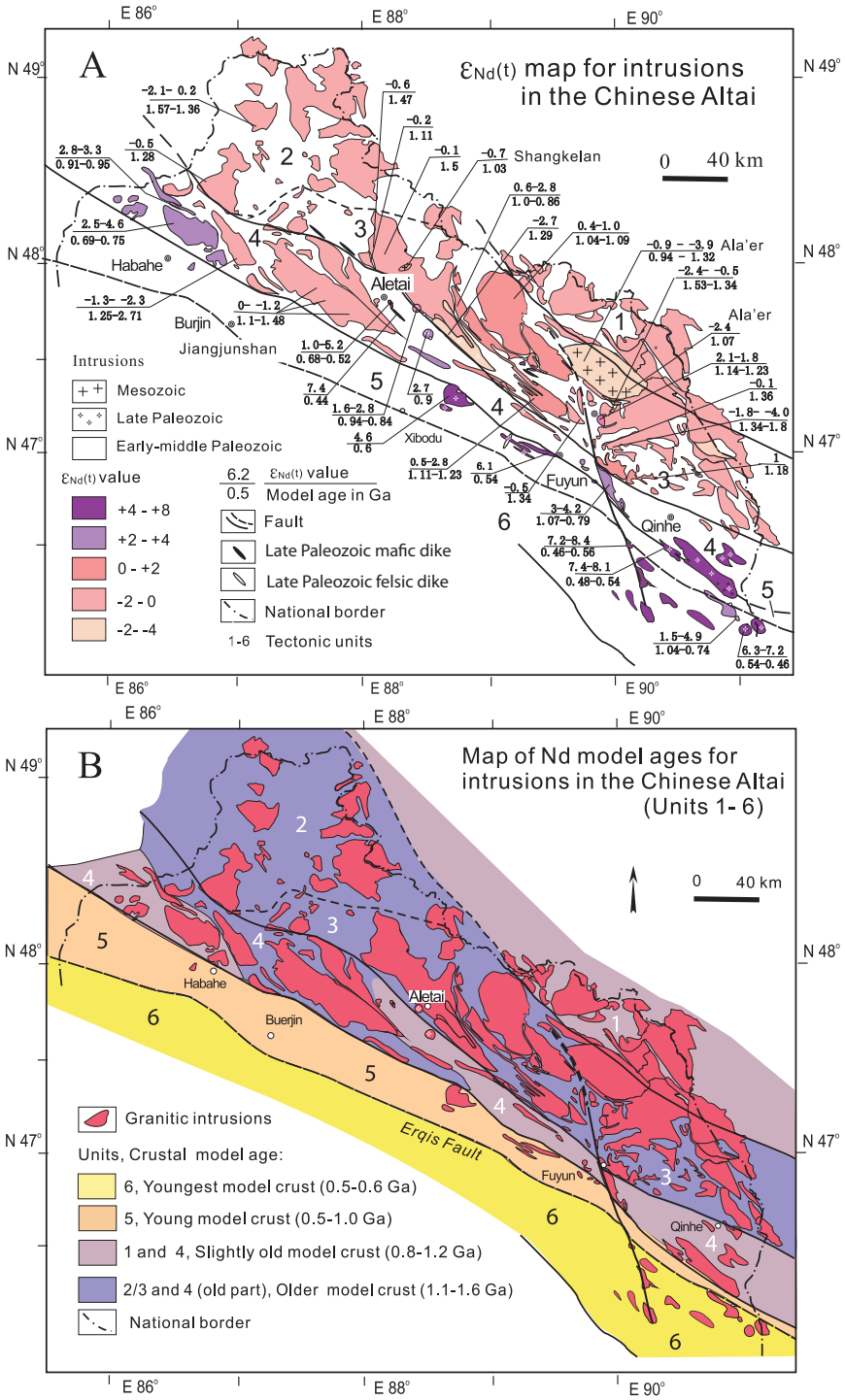

Fig. 11. Isotopic mapping of the intrusions in the Chinese Altai. Maps of (A) $\varepsilon_{Nd}(t)$ values and (B) Nd model ages. This figure illustrates the ages of granitoid source regions beneath the various terranes. Units with similar basement with respect to isotopic composition and model age are shown by the same colour or pattern. The model ages shown here are mainly calculated using the one-stage model. A few highly differentiated rocks with strong Sm/Nd fractionation are shown with their two stage model ages (see Wang and others, 2009a for details)

granites could not have been produced by melting of these rocks. Consequently, the Jiangjunshan granites were likely derived from a mixed source composed of juvenile mantle-derived materials and a small amount of an old crustal source.

The proportion of mantle-derived component in the generation of the granitoids from each pluton can be estimated using a simple two-component mixing model, assuming that the crustal component (end-member 1) is represented by the old (Proterozoic-Paleozoic) metamorphic rocks in the Altai. Sm-Nd isotopic compositions for 12 Proterozoic felsic metamorphic rocks (gneisses) in the Altai have been obtained by Hu and others (2000), and all these data are recalculated at 210 Ma, giving an average of $\varepsilon_{Nd}(210) = -5.1$ and Nd = 42.7 ppm. Chen and Jahn (2002) also measured 10 Paleozoic felsic metamorphic rocks (gneisses and schists) in the Altai, and these yield an average of $\varepsilon_{Nd}(210) = -5.6$ and Nd = 24.9 ppm. Thus, a crude average of all these data give $\varepsilon_{Nd}(210) = -5.4$ and Nd = 33.8 ppm, which is considered to be the crustal component (end-member 1) in the Chinese Altai. The middle Paleozoic Kuerti ophiolite in the Altai (Xu and others, 2003) happens to have the same isotopic characteristics as depleted mantle-derived basalt ($\varepsilon_{Nd}(400) = +8$, Nd = 15 ppm; Jahn and others, 2000a, 2000b), thus, $\varepsilon_{Nd}(210) = +6$ and Nd = 15 ppm are taken as the mantle-derived component (end-member 2). Based on these assumptions, a mixing calculation yielding the proportion of mantle-derived component for the Ala'er, Shangkelan and Jiangjunshan intrusions was *ca.* 40 to 56 percent, *ca.* 58 percent and *ca.* 70 to 90 percent, respectively (table 3).

Based on the previous discussion, we suggest that underplated mafic magma might provide not only the necessary heat source for the melting of both old continental and young juvenile materials, but also contributed to the melts. This is supported by high positive whole-rock $\varepsilon_{Nd}(t)$ and zircon $\varepsilon_{Hf}(t)$ values of some of the Mesozoic granites in the Chinese Altai and Nd-Hf decoupling in the granites, such as those from the Shangkelan pluton (fig. 7). The compositions of the individual terranes have probably controlled the proportion of old crustal and young juvenile mantle-derived components in the production of the various granites. The Mesozoic granites with A-type features were probably produced by an advanced degree of differentiation.

A few isotopic data have been published on the granitic intrusions from the Russian and Kazakstan Altai. These granites are associated with coeval mafic intrusions, thus, they likely contain a higher proportion of mantle-derived components. It has been suggested that the early Mesozoic magmatism in the Russian Altai is related to the activity of the Siberian superplume, which peaked at 252 to 248 Ma (Vladimirov and others, 2008; Buslov and others, 2010).

Finally, the Mesozoic intrusions in the Altai are commonly associated with significant mineral deposits. For example, the early Mesozoic Kalguty granite-leucogranite complex of the Russian Altai (216 ± 3 Ma, $\varepsilon_{Nd}(t)$ values = −1.9 to −5.1) is accompanied by W-Mo-Bi-Be mineralization (Annikova and others, 2006). The pegmatitic veins in the Chinese Altai are also known to contain the W-Mo-Bi-Be mineralization (Han, 2008). Alkaline mafic magmatism is intimately associated with widespread Ag-Sb (about 240 Ma) and Cu-Ag-Sb-Hg (234 ± 1 Ma, sericite Ar-Ar age) mineralization in the Mongolian Altai. This was interpreted as the metallogenic signature of a mantle plume (Pavlova and others, 2008).

Tectonic Setting and Significance

The Mesozoic intrusions in the Chinese Altai show no deformation along their margins or of the contact aureole. Moreover, they are discordant with the country rock stratigraphy, regional foliations and tectonic trends in the host rocks. Such structural patterns suggest they were post-tectonic and were passively emplaced in an extensional tectonic setting. In addition, their shoshonitic and A-type granitic geochemical characteristics suggest a within-plate (or post-orogenic) extensional setting (for example, Yb

vs. Ta and Rb vs. Yb + Ta diagrams, not shown here), although the tectonic implications based on the geochemistry may not be strictly valid because highly differentiated granites show the REE tetrad effect and non-CHARAC trace element behavior, many studies on the regional tectonic evolution consistently suggest that the major orogenic activities (437-375 Ma) in the Altai orogen were terminated in the late Paleozoic (290-270 Ma) and that the tectonic setting became post-orogenic or post-accretionary after this time (Wang and others, 2005, 2006, 2010). Therefore, the early Mesozoic plutons were most likely emplaced in an intraplate anorogenic setting.

The early Mesozoic intraplate anorogenic setting of the Altai orogen is also supported by the regional early Mesozoic magmatic assemblages. In the Gorny Altai of southern Siberia, Early Mesozoic Chuya mafic intrusions, including high-K lamprophyres and syenites, were emplaced in two periods (250-243 and 237-235 Ma, Vasyukova and others, 2011). The association of these intrusions indicates an extensional setting. Furthermore, in the northern part of the Altai-Sayan Fold Area, Triassic basaltic flows and sills were emplaced at 250 to 248 Ma (Buslov and others, 2010). These basalts are medium- to high-Ti tholeiites and they could be linked with the Permo–Triassic flood basalts of the Siberian Platform (Siberian Traps), produced by the activity of the Siberian superplume at 252 to 248 Ma (Buslov and others, 2010). The abrupt change of thickness in the Kuznetsk Late Permian to Middle Triassic units suggests that their formation within an extensional regime was similar to the exposed rifts in the Southern Urals and northern Mongolia and the buried rifts of the West Siberian Basin. Consequently, early Mesozoic intraplate anorogenic magmatism in the Altai appears to be related to a far-field effect of the Siberian superplume (252-248 Ma), with the magmatism appearing to be younging from the northeast (southern Siberia) to the southwest (Altai).

Outside of the Altai Orogen, early Mesozoic granites occur widely in the eastern part of the CAOB, such as in Transbaikalia, NE Mongolia and NE China (Wu and others, 2000; Yarmolyuk and others, 2002, 2008; Yakubchuk, 2004; Vorontsov and others, 2007; Li and others, 2007; Jahn and others, 2009). Some of these granites are syn-orogenic and some are post-orogenic. They were probably related to Mesozoic subduction/collision, such as the Transbaikalian arc, the Mongol-Okhotsk suture, and the Circum-Pacific arcs (Yarmolyuk and others, 2002; Yakubchuk, 2004).

However, in several regions of the central part of the CAOB, including central Mongolia (Yarmolyuk and others, 2002), southern Mongolia near the border with China (Wang and others, 2004), and at Beishan in NW China (Li and others, 2012), the early Mesozoic intrusions (240-210 Ma) were probably emplaced in an intraplate- or post-orogenic extensional setting. The Triassic granitoids (237-229 Ma) occurring along the southern margin of the CAOB in Inner Mongolia were thought to be emplaced in a post-collisional setting (Li and others, 2007). Recently, Li and others (2010, 2013) considered that the early Mesozoic intrusions along the southern margin of the CAOB occurred in two stages: in the Early-Middle Triassic (250-230 Ma) and in the Late Triassic (230-190 Ma). The first-stage intrusions show a high calc-alkaline affinity, and were emplaced in a post-collisional setting, whereas the second stage intrusions have bimodal affinities (associated with lamprophyre dikes) and were emplaced in a post-orogenic extensional setting.

In summary, the early Mesozoic granites show different characteristics and tectonic settings in the western and eastern parts of the CAOB. Syn-orogenic Mesozoic granitoids are widespread and voluminous in the eastern part and southeastern margin of the CAOB. This could be due to the progressive closure, from west to east, of the Paleo-Asian Ocean, and/or subduction of the Mongol-Okhotsk Ocean, as well as subduction of the Paleo-Pacific Ocean to the east. The early Mesozoic intraplate anorogenic granitoids in the western part of the CAOB, however, appear to be related

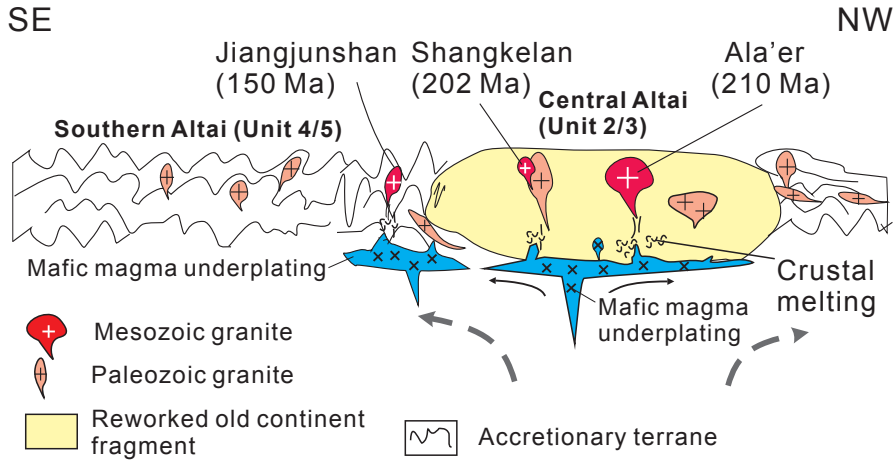

Fig. 12. Cartoon showing the accretionary crustal architecture and tectonic setting of the Mesozoic granites in the Chinese Altai. Underplating of mafic magma heated the base of the lower crust, generating the granitic magmas. Both the long-lived crustal rocks and a juvenile component contributed to the magma. The granites (the Ala'er and Shangkelan granites) in the central Altai (old terrane) contain more long-lived crustal components than those (the Jiangjunshan granite) in the southern Altai (young accretionary terrane). The basement of both terranes has retained its original nature, and the Altai orogen kept its original architecture of Paleozoic horizontal accretion during the Mesozoic.

to a far-field effect of the Siberian superplume (252-248 Ma). One reason is that the Paleo-Asian Ocean had closed by the Late Permian (Xiao and others, 2008) and the Mongol-Okhotsk Ocean was small at that time and its far-field effect might be expected to be weak.

Implications for Crustal Architecture and Continental Growth

In the central Altai microcontinent (Unit 3, fig. 1), the isotopic signatures (negative $\varepsilon_{Nd}(t)$ values) of the Mesozoic anorogenic granites are similar to those of the Paleozoic syn-orogenic granitoids (Wang and others, 2006, 2009a). This implies that the basement of the terrane retained its original continental signature (and was not modified by juvenile mantle-derived material during the Mesozoic). Likewise, the Nd isotopic compositions of the Mesozoic granites in the southern Altai (Unit 4) are similar to those of the Paleozoic syn- and post-orogenic granitoids. Thus, the basement of this terrane has also retained its original juvenile nature (Wang and others, 2006, 2009a). Figure 12 shows the general architecture of the Chinese Altai orogen. The original Paleozoic horizontal accretion was retained in Mesozoic time, and the older continental terrane was not thrust onto, or subducted beneath, the younger juvenile accretionary terrane, as seen in some collisional orogens. Such crustal architecture in the Altai is typical of an accretionary orogen that is characterized by horizontal accretion, not by vertical superposition of terranes.

It is now well established that the CAOB represents the most important site of crustal growth in the Phanerozoic (Sengör and others, 1993; Jahn and others, 2000a, 2000b, 2004; Kovalenko and others, 2004). Crustal growth can be achieved by both lateral and vertical accretion of juvenile material. The emplacement of large volumes of post-accretionary granites with juvenile sources reflects vertical crustal growth, due most likely to a series of processes, including underplating of basaltic magma, mixing of basaltic magmas or melts with lower-crustal rocks, partial melting of the mixed lithologies leading to generation of granitic liquids, and followed by fractional crystallization (Jahn, 2004).

However, Kröner and others (2013) emphasized the importance of remelting or recycling of older crustal material in the generation of Paleozoic granitoids in the CAOB and argued that the production of mantle-derived or juvenile continental crust during the accretionary history of the Central Asian Orogenic Belt (CAOB) has been overestimated. These authors are correct in pointing out the important role of recycling of older crustal material in the generation of syn-orogenic granitoids. However, in their assessment, post-orogenic granitoids are entirely excluded. This is in contrast with the assessment made by other authors (for example, Jahn and others, 2000a, 2000b, 2004; Kovalenko and others, 2004). In the studies of these workers, all the juvenile crustal rocks produced within the CAOB are considered, regardless of whether they are syn-, post- or an-orogenic intrusions. The Mesozoic juvenile granitoids from the CAOB and also from NE China (the "Manchurides" of Sengor and others, 1993) are also included.

Specific to the present study, the early Mesozoic granites in the central Altai were indeed mainly derived from recycling of an old terrane (Units 2 and 3), but the Mesozoic granites in the southern Altai (Units 4 and 5) could not have been entirely produced by crustal remelting at depth; they require additional juvenile, mantle-derived material as well. Thus, vertical crustal growth had to occur in the Mesozoic anorogenic setting of the Altai orogeny.

CONCLUSIONS

The present study leads to the following conclusions:

1. Two distinct Mesozoic granitic intrusive events have been identified in the Chinese Altai orogen. The first occurred in the Late Triassic (220-200 Ma) and was represented by intrusions of albite granite, two-mica monzogranite, biotite monzogranite and late-stage pegmatites. This event is comparable with the Triassic (240-200 Ma) intrusions, including felsic, mafic and alkaline rocks, in the Russian, Kazakhstan and Mongolian Altai. The second event took place in the Late Jurassic (*ca.* 150 Ma), and was characterized by intrusions of alkali feldspar granite, two-mica monzogranite and garnet muscovite monzogranite, some characterized by the presence of high-Ba amazonite.

2. The Late Triassic (220-200 Ma) granites in the Chinese Altai occur in the central Altai (Unit 3). They are highly differentiated I-types, and have whole-rock $\varepsilon_{Nd}(210)$ values of -0.6 to -4.3 and zircon $\varepsilon_{Hf}(t)$ values of -4.0 to $+8.2$, suggesting that they were derived from a mixed source composed of old continental crust and juvenile mantle-derived materials. The Late Jurassic (*ca.* 150 Ma) granites occur within the young accretionary terrane (Unit 4) in the southern Altai. They have an A-type affinity, show the lanthanide tetrad effect in REE distribution patterns, and have positive $\varepsilon_{Nd}(151)$ values of $+1.0$ to $+5.2$ and $\varepsilon_{Hf}(151\ Ma)$ values of $+1$ to $+8$. They were probably derived by melting of juvenile (mantle-derived) basic rocks.

3. The isotopic signatures of the Mesozoic granites from the central (old terrane) and southern Altai (young accretionary terrane) suggest that the basement of both terranes retained its original nature. This further implies that the Altai orogen has kept its original architecture that was the result of Paleozoic horizontal accretion.

4. The early Mesozoic (Triassic) intrusions in the Altai were emplaced in an intraplate anorogenic setting, probably related to a far-field effect of the Siberian superplume (252-248 Ma). The tectonic setting and geodynamic evolution of the rocks is different between the western (anorogenic) and eastern (syn- or post-orogenic) parts of the CAOB. Such differences could have resulted from the progressive closure, from west to east, of the Paleo-Asian Ocean and Mongol-Okhotsk Ocean, or even be related to Paleo-Pacific Ocean subduction.

ACKNOWLEDGMENTS

The staff members of the SHRIMP Center (Dun-yi Liu and Biao Song) helped in the acquisition of the zircon age data reported here. Bao-fu Han and Deng-hong Wang gave constructive comments. Ivan Kozakov, Alexander B. Kotov and Antonio Castro are thanked for their fruitful discussions and cooperation in the research. The work was financially supported by the Chinese National 973 Program (2001CB409800 and 2013CB429803), the National Natural Science Foundation of China (NSFC grants 40472101 and 40072023), the International Cooperation Project of the NSFC (40211120647, 40472101) and NSC-RFBR (RFBR-06-05-39014, 96WIA0100026, 11-05-92003), the China Geological Survey program (No 1212010611803, 1212011085474 and 1212011120135), and Opening Foundation of The Key Laboratory of Northwest University (Xi'an, China). Bor-ming Jahn acknowledges the support of NSC-Taiwan (NSC99-2119-M-002-026, NSC100-2116-M-002-024, NSC100-2923-M-002-010).

Appendix

analytical methods

U-Pb Zircon Dating

The sensitive high resolution ion microprobe (SHRIMP II) analyses were performed at Curtin University, Australia and at the Beijing SHRIMP Center, China. The SHRIMP analyses at Curtin University were ratioed to the CZ3 standard. Spot sizes averaged ~25 μm and each analysis site was rastered for three minutes to remove any surface contamination. An average mass resolution of ~4700 (1% definition) was used to measure Pb/Pb and Pb/U isotopic ratios and Pb/U ratios were normalized to those measured on the standard zircon [CZ3 − ($^{206}Pb/^{238}U$ = 0.0914)]. The coefficient of variation in Pb/U isotopic ratios measured on the CZ3 standard was 2.2 percent during the analytical session. Measured ^{204}Pb count rates on the unknowns were similar to those obtained from the standard zircon and so common lead corrections were made assuming an isotopic composition of Broken Hill lead, since the common lead is considered to be associated mainly with surface contamination in the gold coating (Nelson, 1997). The $^{206}Pb/^{238}U$ ages are generally considered more precise for concordant Phanerozoic zircons (Compston and others, 1992), because low count rates on ^{207}Pb result in large statistical uncertainties, making the $^{207}Pb/^{206}Pb$ and $^{207}Pb/^{235}U$ ratios less sensitive measures of age. U-Pb isotope age data were calculated and plotted using the ISOPLOT (Ludwig, 2003) and SQUID (1.02) software of Ludwig (2003). Uncertainties on individual analyses are quoted at the 1 level, whereas the pooled analyses are quoted at 2σ or 95 percent confidence level.

The analytical techniques in the Beijing SHRIMP Center were basically the same as those at Curtin University. U-Th-Pb isotopic ratios were determined relative to the TEMORA standard zircon (Black and others, 2003), and the U, Th and Pb concentrations were calibrated relative to SL13 reference zircon (U content 238 ppm; age 572 Ma). Zircon grains were mounted in epoxy, together with TEMORA (417 Ma) and the mount was polished to expose zircon internal sections. Cathodoluminescence (CL) imaging was conducted for each grain on a JEOL scanning electron microscope. U-Pb isotope age data were calculated and plotted using the ISOPLOT (Ludwig, 2003) and SQUID (1.02) software of Ludwig (2003). The analytical data are presented with 1σ error boxes on the concordia plots, and the uncertainties in weighted mean ages are quoted at the 95 percent confidence level (2σ). The decay constants used in age calculation are $^{238}U = 0.155125\ Ga^{-1}$ and $^{235}U = 0.98485\ Ga^{-1}$.

U-Pb TIMS analyses were undertaken at the Institute of Precambrian Geology and Geochronology (IPGG), Russian Academy of Sciences, St. Petersburg, using a Finnigan MAT-261 mass-spectrometer. Handpicked multigrain zircon fractions, consisting of 20 to 200 grains, were dissolved and chemically separated following the method of Krogh (1973). Before dissolution, zircon grains were ultrasonically washed in alcohol and acetone. Additional soft acid washing to eliminate surface contamination was performed using warm 1M HNO_3 and warm 1:1 HCL for 20 minutes each. All samples were spiked with a ^{235}U-^{208}Pb mixed tracer. Total blanks were 10 to 50 pg Pb and 1 to 5 pg U. The PBDAT (Ludwig, 1991) and ISOPLOT (Ludwig, 2003) programs were used for the data reduction, including calculation of uncertainties, correlations of U/Pb ratios, regression lines and concordia intercept ages. All errors are reported at the 2 sigma level. The decay constants are the same as mentioned above, and the corrections for common Pb were made using the values of Stacey and Kramers (1975).

LA-ICPMS was also used for zircon dating at the Key Laboratory of Continental Dynamics of Northwest University, Xi'an, and at the Tianjin Institute of Geology and Mineral Resources, Tianjin, China. A detailed

description of the instrumentation, working parameters and calibration procedures is given by Yuan and others (2004). The NIST SRM610 standard glass was used for internal calibration at the Key Laboratory of Continental Dynamics of Northwest University. The data were acquired in peak-switching-pulse-counting mode with one-point measured per peak. Zircon 91500 was used as the external calibration standard and was measured after every 4 or 5 sample spots. The NIST SRM610 was measured twice before and after analyzing around 20 samples, and ^{29}Si was used as an internal standard for U, Th and Pb analyses. The analyses were obtained using a laser-ablation microprobe (193 nm, GeoLas 200 M) coupled to a Neptune (Thermo Fisher) MC-ICPMS at the Tianjin Institute of Geology and Mineral Resources. NIST 612 glass was used as an internal standard for U, Th and Pb analyses and zircon GJ-1 was used as the external calibration standard.

Geochemical and Isotopic Analysis

Major and trace element analyses were obtained at the Key Laboratory of Continental Dynamics of Northwest University, Xi'an, China. Major oxides were analyzed using X-ray fluorescence (RIX2100X sequential spectrometer) on fused Li-borate glass beads, and BCR-2 and GBW07105 were used as reference materials. The uncertainty of the XRF analyses was better than 5 percent. FeO was determined by the wet chemical titration method. Trace elements were measured by LA-ICPMS (Elan 6100DRC), following the method of Gao and others (1999). USGS standards AGV-1, BCR-1 and BHVO-1 were used for calibration. The analytical uncertainties are better than 5 percent for Co, Ni, Zn, Ga, Rb, Y, Zr, Nb, Hf, Ta and LREE, and 5 percent to 15 percent for the others. Major and trace element analyses for the samples AT-1 and AT-2 were obtained at National Taiwan University. Major and trace elements of samples 3211, 32112, 3141-A, 3141-B, 3142 and 3146 were analyzed at Acme Analytical Laboratories (Vancouver) Ltd. Major elements and Zr were analyzed by inductively coupled plasma (ICP) emission spectrometry following a lithium metaborate/tetraborate fusion and dilution. Trace element and rare-earth elements (REE) were analyzed by ICP mass spectrometry.

Nd-Sr isotopes were analyzed by isotope dilution at the Institute of Precambrian Geology and Geochronology, Russian Academy of Sciences, St. Petersburg. Rock powders were dissolved in a mixture of HF, HNO_3 and $HClO_4$. Before decomposition, all samples were spiked with ^{149}Sm-^{150}Nd and ^{85}Rb-^{84}Sr mixed solutions. REE, Rb and Sr were separated using BioRad AG1-X8 200–400 mesh resin using conventional cation-exchange techniques. Sm and Nd were separated by extraction chromatography on LN-Spec (100-150 mesh) resin. Total blanks in the laboratory were 0.1–0.2 ng for Sm, 0.1–0.5 ng for Nd, 0.01–0.05 ng for Rb and 0.3–0.7 ng for Sr. Isotopic compositions of Sm, Nd, Rb and Sr were measured on a Triton TI multi-collector mass-spectrometer in static mode. The measured ratios of $^{87}Sr/^{86}Sr$ and $^{143}Nd/^{144}Nd$ were normalized to $^{86}Sr/^{88}Sr = 0.1194$ and $^{146}Nd/^{144}Nd = 0.7219$, respectively. The accuracy of the measurements of Sm, Nd, Rb and Sr concentrations were ±0.5%, $^{147}Sm/^{144}Nd = \pm 0.5\%$, $^{143}Nd/^{144}Nd = \pm 0.005\%$, $^{87}Rb/^{86}Sr = 0.5\%$, $^{87}Sr^{86}Sr = 0.05\%$ (2σ). $^{143}Nd/^{144}Nd$ ratios were adjusted to the value of 0.511860 for the La Jolla Nd standard. During the period of analysis, the weighted average of 5 La Jolla Nd-standard runs yielded 0.511844 ± 3 (2σ) for $^{143}Nd/^{144}Nd$.

The $\varepsilon_{Nd}(t)$ values were calculated using the present-day values for a chondritic uniform reservoir (CHUR) $^{143}Nd/^{144}Nd = 0.512638$ and $^{147}Sm/^{144}Nd = 0.1967$. Sm-Nd model ages were calculated in two ways. The one-stage model age (T_{DM1}) was calculated assuming a linear Nd isotopic growth of the depleted mantle reservoir from $\varepsilon_{Nd} = 0$ at 4.56 Ga to $\varepsilon_{Nd} = +10$ at present. The two-stage model age, which is applied for samples that have $^{147}Sm/^{144}Nd$ ratios larger than 0.14 or $f_{Sm/Nd}$ ratios > -0.2 or < -0.6, was obtained assuming that the protolith of the granitic magmas had a Sm/Nd ratio (or $f_{Sm/Nd}$ value) of the average continental crust (Keto and Jacobsen, 1987). The calculation formulas, as well as analytical precision, Sr-Nd isotope standard and normalization values, and blank levels can be found in the footnotes to table 3.

In-situ Zircon Hf Isotopic Analyses

In-situ zircon Hf isotope analyses were carried out using a Newwave UP213 laser-ablation microprobe, attached to a Neptune multi-collector ICP-MS at the Institute of Mineral Resources, Chinese Academy of Geological Sciences, Beijing. Instrumental conditions and data acquisition were as described by Hou and others (2007) and Wu and others (2006). A spot with a beam diameter of either 40 μm or 55 μm was selected depending on the size of the ablated domains. Helium was used as the carrier gas to transport the ablated sample from the laser-ablation cell to the ICP-MS torch and was mixed with argon. In order to correct the isobaric interferences of ^{176}Lu and ^{176}Yb on ^{176}Hf, $^{176}Lu/^{175}Lu = 0.02658$ and $^{176}Yb/^{173}Yb = 0.796218$ ratios were determined (Chu and others, 2002). For instrumental mass bias correction Yb isotope ratios were normalized to $^{172}Yb/^{173}Yb = 1.35274$ (Chu and others, 2002) and Hf isotope ratios to $^{179}Hf/^{177}Hf = 0.7325$ using an exponential law. The mass bias behavior of Lu was assumed to follow that of Yb, and mass bias correction protocols are as described in Wu and others (2006) and Hou and others (2007). Zircons GJ1 and

Pušovice were used as the reference standards during analyses, with a weighted mean $^{176}Hf/^{177}Hf$ ratio of 0.282007 ± 0.000007 (2σ, n = 36) and 0.282476 ± 0.000004 (2σ, n = 27), respectively. These are indistinguishable from the weighted mean $^{176}Hf/^{177}Hf$ ratio of 0.282000 ± 0.000005 (2σ) and 0.282482 ± 0.000008 (2σ), respectively, determined using the solution analysis method by Morel and others (2008) and Slama and others (2008).

References

Annikova, I., Vladimirov, A., Vystavnoi, S., Zhuravlev, D., Kruk, N., Lepekhina, E., Matukov, D., Moroz, E., Palesskii, S., Ponomarchuk, V., Rudnev, S., and Sergeev, S., 2006, U-Pb and $^{39}Ar/^{40}Ar$ dating and Sm-Nd and Pb-Pb isotopic study of the Kalguty molybdenum-tungsten ore-magmatic system (Southern Altai): Petrology, v. 14, n. 1, p. 81–97, http://dx.doi.org/10.1134/S0869591106010073

Badarch, G., Cunningham, W. D., and Windley, B. F., 2002, A new terrane subdivision for Mongolia: implications for the Phanerozoic crustal growth of Central Asia: Journal of Asian Earth Sciences, v. 21, n. 1, p. 87–110, http://dx.doi.org/10.1016/S1367-9120(02)00017-2

Bau, M., 1996, Controls on the fractionation of isovalent trace elements in magmatic and aqueous systems: evidence from Y/Ho, Zr/Hf, and lanthanide tetrad effect: Contributions to Mineralogy and Petrology, v. 123, n. 3, p. 323–333, http://dx.doi.org/10.1007/s004100050159

Black, L. P., Kamo, S. L., Williams, I. S., Mundil, R., Davis, D. W., Korsch, R. J., and Foudoulis, C., 2003, The application of SHRIMP to Phanerozoic geochronology; a critical appraisal of four zircon standards: Chemical Geology, v. 200, n. 1–2, p. 171–188, http://dx.doi.org/10.1016/S0009-2541(03)00166-9

Briggs, S. M., Yin, A., Manning, C. E., Chen, Z. L., and Wang, X. F., 2009, Tectonic development of the southern Chinese Altai Range as determined by structural geology, thermobarometry, $^{40}Ar/^{39}Ar$ thermochronology, and Th/Pb ion-microprobe monazite geochronology: Geological Society of America Bulletin, v. 121, n. 9–10, p. 1381–1393, http://dx.doi.org/10.1130/B26385.1

Buslov, M. M., Safonova, I. Y., Fedoseev, G. S., Reichow, M. K., Davies, K., and Babin, G. A., 2010, Permo-Triassic plume magmatism of the Kuznetsk Basin, Central Asia: geology, geochronology, and geochemistry: Russian Geology and Geophysics, v. 51, n. 9, p. 1021–1036, http://dx.doi.org/10.1016/j.rgg.2010.08.010

Chappell, B. W., and White, A. J. R., 1992, I- and S-type granites in the Lachlan Fold Belt: Transactions of the Royal Society of Edinburgh: Earth Sciences, v. 83, n. 1–2, p. 1–26, http://dx.doi.org/10.1017/S0263593300007720

Chen, B., and Jahn, B. M., 2002, Geochemical and isotopic studies of the sedimentary and granitic rocks of the Altai orogen of northwest China and their tectonic implications: Geological Magazine, v. 139, n. 1, p. 1–13, http://dx.doi.org/10.1017/S0016756801006100

——— 2004, Genesis of post-collisional granitoids and basement nature of the Junggar Terrane, NW China: Nd-Sr isotope and trace element evidence: Journal of Asian Earth Sciences, v. 23, n. 5, p. 691–703, http://dx.doi.org/10.1016/S1367-9120(03)00118-4

Chen, F., Li, H., Wang, D., Cai, H., and Chen, W., 2000, New chronological evidence for Yanshanian diagenetic mineralization in China's Altay orogenic belt: Chinese Science Bulletin, v. 45, n. 2, p. 108–114, http://dx.doi.org/10.1007/BF02884652

Chu, N. C., Taylor, R. N., Chavagnac, V., Nesbitt, R. W., Boella, R. M., Milton, J. A., German, C. R., Bayon, G., and Burton, K., 2002, Hf isotope ratio analysis using multi-collector inductively coupled plasma mass spectrometry: an evaluation of isobaric interference corrections: Journal of Analytical Atomic Spectrometry, v. 17, p. 1567–1574, http://dx.doi.org/10.1039/b206707b

Coleman, R. G., 1989, Continental growth of Northwest China: Tectonics, v. 8, n. 3, p. 621–635, http://dx.doi.org/10.1029/TC008i003p00621

Compston, W., Williams, I. S., Kirschvink, J. L., Zhang, Z., and Guogan, M. A., 1992, Zircon U-Pb ages for the Early Cambrian timescale: Journal of the Geological Society, London, v. 149, n. 2, p. 171–184, http://dx.doi.org/10.1144/gsjgs.149.2.0171

Demin, A. N., Demin, P. A., and Andreev, V. V., 2001, Early Mesozoic ore-bearing granitoids and their tectonic setting in the Mongolian Altay. Postcollisional Evolution of Mobile Belts: Irkutsk, Abstracts, International Conference, VII A. N. Zavaritsky Memorial Workshop [in Russian].

Dokukina, K. A., Konilov, A. N., Kaulina, T. V., and Vladimirov, V. G., 2010, Interaction between mafic and felsic magmas in subvolcanic environment (Tastau igneous complex, eastern Kazakhstan): Russian Geology and Geophysics, v. 51, n. 6, p. 625–643, http://dx.doi.org/10.1016/j.rgg.2010.05.004

Gao, S., Ling, W., Qiu, Y., Lian, Z., Hartmann, G., and Simon, K., 1999, Contrasting geochemical and Sm-Nd isotopic compositions of Archean metasediments from the Kongling high-grade terrain of the Yangtze craton: Evidence for cratonic evolution and redistribution of REE during crustal anatexis: Geochimica et Cosmochimica Acta, v. 63, n. 13–14, p. 2071–2088, http://dx.doi.org/10.1016/S0016-7037(99)00153-2

Gusev, A. I., 2004, Petrology of gold-generating granitoids, *in* Khanchuk, A. I., Gonevchuk, G. A., Mitrokhin, A. N., Simanenko, L. F., Cook N. J., and Seltmann, R., editors, Metallogeny of the Pacific Northwest (Russian Far East): Tectonics, Magmatism and Metallogeny of Active Continental Margins, Guidebook for the Field Excursions in the Far East of Russia, September 1–20, 2004: Vladivostok, Dalnauka, Far Eastern Geological Institute, Russian Federation, p. 206–209.

Han, B. F., 2008, A preliminary comparison of Mesozoic granitoids and rare metal deposits in Chinese and Russian Altai Mountains: Acta Petrologica Sinica, v. 24, n. 4, p. 655–660.

Han, B. F., Guo, Z. J., Zhang, Z. C., Zhang, L., Chen, J. F., and Song, B., 2010, Age, geochemistry, and tectonic implications of a late Paleozoic stitching pluton in the North Tian Shan suture zone, western

China: Geological Society of America Bulletin, v. 122, n. 3–4, p. 627–640, http://dx.doi.org/10.1130/B26491.1

He, G. Q., Han, B. F., Yue, Y. J., and Wang, J. H., 1990, Tectonic division and crustal evolution of Altay Orogenic Belt in China: Geoscience (Xinjiang), v. 2, p. 9–20.

He, G. Q., Li, M. S., Liu, D. Q., and Zhou, N. H., 1994, Palaeozoic Crustal Evolution and Mineralization in Xinjiang of China: Urumqi, Xinjiang People's Publishing House, p. 1–437.

Hou, K. J., Li, Y. H., Zou, T. R., Qu, X. M., Shi, Y. R., and Xie, G. Q., 2007, Laser ablation-MC-ICP-MS technique for Hf isotope microanalysis of zircon and its geological applications: Acta Petrologica Sinica, v. 23, p. 2595–2604.

Hu, A. Q., Wang, Z. G., and Tu, G. Z., 1997, Geological evolution and metallogenetic regularity in Northern Xinjiang: Beijing, Science Press, p. 52–62 (in Chinese).

Hu, A. Q., Jahn, B. M., Zhang, G. X., Chen, Y. B., and Zhang, Q. F., 2000, Crustal evolution and Phanerozoic crustal growth in northern Xinjiang: Nd isotopic evidence, Part I. Isotopic characteristics of basement rocks: Tectonophysics, v. 328, n. 1–2, p. 15–51, http://dx.doi.org/10.1016/S0040-1951(00)00176-1

Irber, W., 1999, The lanthanide tetrad effect and its correlation with K/Rb, Eu/Eu*, Sr/Eu, Y/Ho, and Zr/Hf of evolving peraluminous granite suites: Geochimica et Cosmochimica Acta, v. 63, n. 3–4, p. 489–508, http://dx.doi.org/10.1016/S0016-7037(99)00027-7

Jahn, B. M., 2004, The Central Asian Orogenic Belt and growth of the continental crust in the Phanerozoic: Geological Society, London, Special Publications, v. 226, p. 73–100, http://dx.doi.org/10.1144/GSL.SP.2004.226.01.05

Jahn, B. M., Wu, F. Y., and Chen, B., 2000a, Granitoids of the Central Asian Orogenic Belt and continental growth in the Phanerozoic: Transactions of the Royal Society of Edinburgh: Earth Sciences, v. 91, n. 1–2, p. 181–193, http://dx.doi.org/10.1017/S0263593300007367

——— 2000b, Massive granitoid generation in central Asia: Nd isotopic evidence and implication for continental growth in the Phanerozoic: Episodes, v. 23, p. 82–92.

Jahn, B. M., Wu, F., Capdevila, R., Martineau, F., Zhao, Z., and Wang, Y., 2001, Highly evolved juvenile granites with tetrad REE patterns: The Woduhe and Baerzhe granites from the Great Xing'an (Khingan) Mountains in NE China: Lithos, v. 59, n. 4, p. 171–198, http://dx.doi.org/10.1016/S0024-4937(01)00066-4

Jahn, B. M., Capdevila, R., Liu, D., Vernon, A., and Badarch, G., 2004, Sources of Phanerozoic granitoids in the transect Bayanhongor–Ulaan Baatar, Mongolia: geochemical and Nd isotopic evidence, and implications for Phanerozoic crustal growth: Journal of Asian Earth Sciences, v. 23, n. 5, p. 629–653, http://dx.doi.org/10.1016/S1367-9120(03)00125-1

Jahn, B. M., Litvinovsky, B., Zanvilevich, A. N., and Reichow, M., 2009, Peralkaline granitoid magmatism in the Mongolian-Transbaikalian Belt: Evolution, petrogenesis and tectonic significance: Lithos, v. 113, n. 3–4, p. 521–539, http://dx.doi.org/10.1016/j.lithos.2009.06.015

Keto, L. S., and Jacobsen, S. B., 1987, Nd and Sr isotopic variations of Early Palaeozoic oceans: Earth and Planetary Science Letters, v. 84, n. 1, p. 27–41, http://dx.doi.org/10.1016/0012-821X(87)90173-7

Kovach, V., Sal'nikova, E., Wang, K. L., Jahn, B. M., Chiu, H. Y., Reznitskiy, L., Kotov, A., Iizuka, Y., and Chung, S. L., 2013, Zircon ages and Hf isotopic constraints on sources of clastic metasediments of the Slyudyansky high-grade complex, southeastern Siberia: Implication for continental growth and evolution of the Central Asian Orogenic Belt: Journal of Asian Earth Sciences, v. 62, p. 18–36, http://dx.doi.org/10.1016/j.jseaes.2011.08.008

Kovalenko, V. I., Yarmolyuk, V. V., Kovach, V. P., Kotov, A. B., and Sal'nikova, E. B., 2003a, Magmatism and geodynamics of Early Caledonian structures of the Central Asian Fold Belt (isotopic and geological data): Russian Geology and Geophysics, v. 44, n. 12, p. 1235–1248.

Kovalenko, V. I., Yarmolyuk, V. V., Sal'nikova, E. B., Budnikov, S. V., Kovach, V. P., Kotov, A. B., Ponomarchuk, V. A., Kozlov, V. D., and Vladykin N. V., 2003b, Sources of Igneous Rocks and Genesis of the Early Mesozoic Tectonomagmatic Area of the Mongolia-Transbaikalia Magmatic Region: 1. Geology and Isotope Geochronology: Petrology, v. 11, n. 2, p. 147–160.

Kovalenko, V. I., Yarmolyuk, V. V., Sal'nikova, E. B., Budnikov, S. V., Kovach, V. P., Kotov, A. B., Ponomarchuk, V. A., Kozlov, V. D., Vladykin, N. V., and Khanchuk, A. I., 2003c, Sources of igneous rocks and genesis of the Early Mesozoic tectonomagmatic area of the Mongolia-Transbaikalia magmatic region: 2. Petrology and geochemistry: Petrology, v. 11, n. 3, p. 205–229.

Kovalenko, V. I., Yarmolyuk, V. V., Kovach, V. P., Kotov, A. B., Kozakov, I. K., Sal'nikova, E. B., and Larin, A. M., 2004, Isotope provinces, mechanisms of generation and sources of the continental crust in the Central Asian Mobile Belt: geological and isotopic evidence: Journal of Asian Earth Sciences, v. 23, n. 5, p. 605–627, http://dx.doi.org/10.1016/S1367-9120(03)00130-5

Kozakov, I. K., Bibikova, E. V., Kovalenko, V. I., Sal'nikova, E. B., Kirnozova, T. I., and Kotov, A. B., 1997, U-Pb age of granitoids located within the southern slope of the Caledonides, Mongolian Altai: Transactions (Doklady) of the Russian Academy of Sciences: Earth Science Sections, v. 353A, n. 3, p. 338–340.

Krogh, T. E., 1973, A low-contamination method for hydrothermal decomposition of zircon and extraction of U and Pb for isotopic age determination: Geochimica et Cosmochimica Acta, v. 37, n. 3, p. 485–494, http://dx.doi.org/10.1016/0016-7037(73)90213-5

——— 1982, Improved accuracy of U-Pb zircon by the creation of more concordant systems using an air abrasion technique: Geochimica et Cosmochimica Acta, v. 46, n. 4, p. 637–649, http://dx.doi.org/10.1016/0016-7037(82)90165-X

Kröner, A., Kovach, V., Belousova, E., Hegner, E., Armstrong, R., Dolgopolova, A., Seltmann, R., Alexeiev, D. V., Hoffmann, J. E., Wong, J., Sun, M., Cai, K., Wang, T., Tong, Y., Wilde, S. A., Degtyarev, K. E., and Rytsk, E., 2013, Reassessment of continental growth during the accretionary history of the Central Asian Orogenic Belt: Gondwana Research, http://dx.doi.org/10.1016/j.gr.2012.12.023

Laurent-Charvet, S., Charvet, J., Monié, P., and Shu, L., 2003, Late Paleozoic strike-slip shear zones in eastern central Asia (NW China): new structural and geochronological data: Tectonics, v. 22, n. 2, 1009, http://dx.doi.org/10. 1029/2001TC901047

Li, J. Y., Xiao, W. J., Wang, K. Z., Sun, G. H., and Gao, L. M., 2003, Neoproterozoic-Paleozoic tectono stratigraphy, magmatic activities and tectonic evolution of eastern Xinjiang, NW China, *in* Mao, J. W., Goldfarb, R. J., Seltman, R., Wang, D. H., Xiao, W. J., and Hart, C., editors, Tectonic Evolution and Metallogeny of the Chinese Altay and Tianshan: London, CERCAM/NHM, IAGOD Guidebook Series 10, p. 31–74.

Li, J. Y., Gao, L. M., Sun, G. H., Li, Y. P., and Wang, Y. B., 2007, Shuangjing middle Triassic syn-collisional crustal derived granite in the east Inner Mongolia and its constraint on the timing of collision between Siberian and Sino-Korean paleo-plates: Acta Petrologica Sinica, v. 23, n. 3, p. 565–582.

Li, S., Wang, T., and Tong, Y., 2010, Spatial-temporal distribution and tectonic setting of Early Mesozoic granitoids in the middle-south segment of the Central Asia Orogenic System: Acta Petrologica et Mineralogica, v. 29, n. 6, p. 642–662.

Li, S., Wang, T., Wilde, S. A., Tong, Y., Hong, D., and Guo, Q., 2012, Geochronology, petrogenesis and tectonic implications of Triassic granitoids from Beishan, NW China: Lithos, v. 134–135, p. 123–145, http://dx.doi.org/10.1016/j.lithos.2011.12.005

Li, S., Wang, T., Wilde, S. A., and Tong, Y., 2013, Evolution, source and tectonic significance of Early Mesozoic granitoid magmatism in the Central Asian Orogenic Belt (central segment): Earth-Science Reviews, http://dx.doi.org/10.1016/j.earscirev.2013.06.001

Litvinovsky, B. A., Jahn, B. M., Zanvilevich, A. N., and Shadaev, M. G., 2002a, Crystal fractionation in the petrogenesis of an alkali monzodiorite-syenite series: the Oshurkovo plutonic sheeted complex, Transbaikalia, Russia: Lithos, v. 64, n. 3–4, p. 97–130, http://dx.doi.org/10.1016/S0024-4937(02)00179-2

Litvinovsky, B. A., Jahn, B. M., Zanvilevich, A. N., Saunders, A., Poulain, S., Kuzmin, D. V., Reichow, M. K., and Titov, A. V., 2002b, Petrogenesis of syenite-granite suites from the Bryansky complex (Transbaikalia, Russia): implications for the origin of A-type granitoid magmas: Chemical Geology, v. 189, n. 1–2, p. 105–133, http://dx.doi.org/10.1016/S0009-2541(02)00142-0

Litvinovsky, B. A., Tsygankov, A. A., Jahn, B. M., Katzir, Y., and Be'eri-Shlevin, Y., 2011, Origin and evolution of overlapping calc-alkaline and alkaline magmas: The Late Palaeozoic post-collisional igneous province of Transbaikalia (Russia): Lithos, v. 125, n. 3–4, p. 845–874, http://dx.doi.org/10.1016/j.lithos.2011.04.007

Liu, W., 1990, Ages and petrogenesis of granitoids in the Altai Mts., Xinjiang, China: Geotectonica et Metallogenia, v. 14, p. 43–56 (in Chinese with English abstract).

Liu, W., Liu, C. Q., and Masuda, A., 1997, Complex trace-element effects of mixing-fractional crystallization composite process: applications to the Ala'er granite pluton, Altay Mountains, Xinjiang, northwestern China: Chemical Geology, v. 135, p. 103–124, http://dx.doi.org/10.1016/S0009-2541(96)00111-8

Long, X. P., Yuan, C., Sun, M., Xiao, W. J., Zhao, G. C., Wang, Y. J., Cai, K. D., Xia, X. P., and Xie, L. W., 2010, Detrital zircon ages and Hf isotopes of the early Paleozoic flysch sequence in the Chinese Altai, NW China: New constrains on depositional age, provenance and tectonic evolution: Tectonophysics, v. 480, n. 1–4, p. 213–231, http://dx.doi.org/10.1016/j.tecto.2009.10.013

Ludwig, K. R., 1991, PbDat for MS-DOS, version 1. 21: U.S. Geological Survey Open-File Report, 88–542, 35 p.

——— 2003, User's Manual for Isoplot 3.00: A geochronological toolkit for Microsoft Excel: Berkeley Geochronology Center, Special Publication, v. 4, p. 25–32.

Maniar, P. D., and Piccoli, P. M., 1989, Tectonic discrimination of granitoids: Geological Society of America Bulletin, v. 101, n. 5, p. 635–643, http://dx.doi.org/10.1130/0016-7606(1989)101⟨0635:TDOG⟩2.3.CO;2

Masuda, A., Nakamura, N., and Tanaka, T., 1973, Fine structures of mutually normalized rare-earth patterns of chondrites: Geochimica et Cosmochimica Acta, v. 37, n. 2, p. 239–248, http://dx.doi.org/10.1016/0016-7037(73)90131-2

Morel, M. L. A., Nebel, O., Nebel-Jacobsen, Y. J., Miller, J. S., and Vroon, P. Z., 2008, Hafnium isotope characterization of the GJ-1 zircon reference material by solution and laser-ablation MC-ICPMS: Chemical Geology, v. 255, n. 1–2, p. 231–235, http://dx.doi.org/10.1016/j.chemgeo.2008.06.040

Nelson, D. R., 1997, Compilation of geochronology data, 1996: Geological Survey of Western Australia, Record, v. 2, 189 p.

Parfenov, L. M., Khanchuk, A. I., Badarch, G., Miller, R. J., Naumova, V. V., Nokleberg, W. J., Ogasawara, M., Prokopiev, A. V., and Yan, H., 2004, Northeast Asia Geodynamic Map: US Geological Survey Open-File Report, 2004-1252.

Pavlova, G. G., Borisenko, A. S., Goverdovskii, V. A., Travin, A. V., Zhukova, I. A., and Tret'yakova, I. G., 2008, Permian-Triassic magmatism and Ag-Sb mineralization in southeastern Altai and northwestern Mongolia: Russian Geology and Geophysics, v. 49, n. 7, p. 545–555, http://dx.doi.org/10.1016/j.rgg.2008.06.010

Peccerillo, R., and Taylor, S. R., 1976, Geochemistry of Eocene calc-alkaline volcanic rocks from the Kastamonu area, northern Turkey: Contributions to Mineralogy and Petrology, v. 58, n. 1, p. 63–81, http://dx.doi.org/10.1007/BF00384745

Scherer, E., Munker, C., and Mezger, K., 2001, Calibration of the lutetium-hafnium clock: Science, v. 293, n. 5530, p. 683–687, http://dx.doi.org/10.1126/science.1061372

Şengör, A. M. C., Natal'in, B. A., and Burtman, V. S., 1993, Evolution of the Altaid tectonic collage and Paleozoic crustal growth in Eurasia: Nature, v. 364, p. 299–307, http://dx.doi.org/10.1038/364299a0

Sláma, J., Košler, J., Condon, D. J., Crowley, J. L., Gerdes, A., Hanchar, J. M., Horstwood, M. S. A., Morris, G. A., Nasdala, L., Norberg, N., Schaltegger, U., Schoene, B., Tubrett, M. N., and Whitehouse, M. J., 2008, Plešovice zircon, a new natural reference material for U/Pb and Hf isotopic microanalysis: Chemical Geology, v. 249, n. 1–2, p. 1–35, http://dx.doi.org/10.1016/j.chemgeo.2007.11.005

Stacey, J. S., and Kramers, I. D., 1975, Approximation of terrestrial lead isotope evolution by a two-stage

model: Earth and Planetary Science Letters, v. 26, n. 2., p. 207–221, http://dx.doi.org/10.1016/0012-821X(75)90088-6

Sun, M., Yuan, C., Xiao, W. J., Long, X. P., Xia, X., Zhao, G. C., Lin, S. F., Wu, F. Y., and Kröner, A., 2008, Zircon U-Pb and Hf isotopic study of gneissic rocks from the Chinese Altai: Progressive accretionary history in the early to middle Palaeozoic: Chemical Geology, v. 247, n. 3–4, p. 352–383, http://dx.doi.org/10.1016/j.chemgeo.2007.10.026

Sun, S. S., and McDonough, W. F., 1989, Chemical and isotopic systematics of oceanic basalts: implications for mantle composition and processes, *in* Saunders, A. D., and Norry, M. J., editors, Magmatism in the Ocean Basins: Geological Society, London, Special Publications, v. 42, p. 313–345, http://dx.doi.org/10.1144/GSL.SP.1989.042.01.19

Sylvester, P. J., 1989, Post-collisional alkaline granitoids: The Journal of Geology, v. 97, n. 3, p. 261–280, http://dx.doi.org/10.1086/629302

Tong, Y., Hong, D. W., Wang, T., Wang, S. G., and Han, B. F., 2006a, TIMS U-Pb zircon ages of Fuyun post-orogenic linear granite plutons on the southern margin of Altay orogenic belt and their implications: Acta Petrologica et Mineralogica, v. 25, n. 2, p. 85–89.

Tong, Y., Wang, T., Kovach, V. P., Hong, D. W., and Han, B. F., 2006b, Age and origin of the Takeshiken postorogenic alkali-rich intrusive rocks in southern Altai, near the Mongolian border in China and its implications for continental growth: Acta Petrologica Sinica, v. 22, n. 5, p. 1267–1278.

Tong, Y., Wang, T., Hong, D. W., Dai, Y. J., Han, B. F., and Liu, X. M., 2007, Ages and origin of the early Devonian granites from the north part of Chinese Altai Mountains and its tectonic implications: Acta Petrologica Sinica, v. 23, n. 8, p. 1933–1944.

Tong, Y., Wang, T., Siebel, W., Hong, D. W., and Sun, M., 2012, Recognition of early Carboniferous alkaline granite in the southern Altai orogen: post-orogenic processes constrained by U-Pb zircon ages, Nd isotopes, and geochemical data: International Journal of Earth Sciences, v. 101, n. 4, p. 937–950, http://dx.doi.org/10.1007/s00531-011-0700-0

Turner, S., Arnaud, N., Liu, J., Rogers, N., Hawkesworth, C., Harris, N., Kelley, S., Van Calsteren, P., and Deng, W., 1996, Post-collision, shoshonitic volcanism on the Tibetan Plateau: implications for convective thinning of the lithosphere and the source of ocean island basalts: Journal of Petrology, v. 37, n. 1, p. 45–71, http://dx.doi.org/10.1093/petrology/37.1.45

Väisänen, M., Mänttäri, I., Kriegsman, L. M., and Holttä, P., 2000, Tectonic setting of post-collisional magmatism in the Palaeoproterozoic Svecofennian Orogen, SW Finland: Lithos, v. 54, n. 1–2, p. 63–81, http://dx.doi.org/10.1016/S0024-4937(00)00018-9

Vasyukova, E. A., Izokh, A. E., Borisenko, A. S., Pavlova, G. G., Sukhorukov, V. P., and Anh, T. T., 2011, Early Mesozoic lamprophyres in Gorny Altai: petrology and age boundaries: Russian Geology and Geophysics, v. 52, n. 12, p. 1574–1591, http://dx.doi.org/10.1016/j.rgg.2011.11.010

Vladimirov, A. G., Ponomareva, A. P., Shokalsky, S. P., Khalilov, V. A., Kostitsyn, Yu. A., Ponomarchuk, V. A., Rudnev, S. N., Vystavnoi, S. A., Kruk, N. N., and Titov, A. V., 1997, Late Paleozoic–Early Mesozoic granitoid magmatism in Altai: Russian Geology and Geophysics, v. 38, n. 4, p. 715–729.

Vladimirov, A. G., Kozlov, M. S., Shokalsky, S. P., Khalilov, V. A., Rudnev, S. N., Kruk, N. N., Vystavnoi, S. A., Borisov, S. M., Berezikov, Y. K., Metsner, A. N., Babin, G. A., Mamlin, A. N., Murzin, O. M., Nazarov, G. V., and Makarov, V. A., 2001, Major epochs of intrusive magmatism of Kuznetsk Alatau, Altai, and Kalba (from U-Pb isotope dates): Geologiya i Geofizika (Russian Geology and Geophysics), v. 42, p. 1157–1178.

Vladimirov, A. G., Kruk, N. N., Polyanskii, O. P., Vladimirov, V. G., Babin, G. A., Rudnev, S. N., Annikova, I. Yu., Travin, A. V., Savinykh, Ya. V., and Palesskii, S. V., 2005, Correlation of Hercynian deformations, sedimentation and magmatism in the Altai collisional system as reflecting plate- and plum-tectonics, *in* Problemy tektoniki Tsentral'noi Azji (Tectonic Problems of Central Asia): Moscow, Geosciences, p. 277–308.

Vladimirov, A. G., Kruk, N. N., Khromykh, S. V., Polyansky, O. P., Chervov, V. V., Vladimirov, V. G., Travin, A. V., Babin, G. A., Kuibida, M. L., and Vladimirov, V. D., 2008, Permian magmatism and lithospheric deformation in the Altai caused by crustal and mantle thermal processes: Russian Geology and Geophysics, v. 49, n. 7, p. 468–479, http://dx.doi.org/10.1016/j.rgg.2008.06.006

Vorontsov, A. A., Yarmolyuk, V. V., Lykhin, D. A., Dril, S. I., Tatarnikov, S. A., and Sandimirova, G. P., 2007, Magmatic sources and geodynamics of the early Mesozoic Northern Mongolia–Western Transbaikalia rift zone: Petrology, v. 15, n. 1, p. 37–60, http://dx.doi.org/10.1134/S0869591107010031

Wang, D. H., Chen, Y. C., Xu, Z. G., Li, T. D., and Fu, X. J., 2002, Mineralogenetic series of mineral deposits and regularity of mineralization in the Altai metallogenic province, Xinjiang, China: Beijing, Atomic Energy Press, p. 1–498 (in Chinese).

Wang, T., Zheng, Y. D., Li, T. B., and Gao, Y. J., 2004, Mesozoic granitic magmatism in extensional tectonics near the Mongolian border in China and its implications for crustal growth: Journal of Asian Earth Sciences, v. 23, n. 5, p. 715–729, http://dx.doi.org/10.1016/S1367-9120(03)00133-0

Wang, T., Hong, D. W., Tong, Y., Wang, Y. B., Han, B. F., and Shi, Y., 2005, Post-orogenic Lamazhao granitic pluton from the Altai orogen, NW China: Acta Petrologica Sinica, v. 21, n. 3, p. 640–650.

Wang, T., Hong, D. W., Jahn, B. M., Tong, Y., Wang, Y. B., Han, B. F., and Wang, W. X., 2006, Timing, petrogenesis and setting of Paleozoic synorogenic intrusions from the Altai Mountains, Northwest China: Implications for the tectonic evolution of an accretionary orogen: The Journal of Geology, v. 114, n. 6, p. 735–751, http://dx.doi.org/10.1086/507617

Wang, T., Tong, Y., Jahn, B. M., Zou, T. R., Wang, Y. B., Hong, D. W., and Han, B. F., 2007, SHRIMP Zircon U-Pb geochronology of No. 3 Pegmatite, NW China, and its implications for the origin and tectonic setting of the pegmatite: Ore Geology Reviews, v. 32, n. 1–2, p. 325–336, http://dx.doi.org/10.1016/j.oregeorev.2006.10.001

Wang, T., Jahn, B. M., Kovach, V. P., Tong, Y., Hong, D. W., and Han, B. F., 2009a, Nd-Sr isotopic mapping of

the Chinese Altai and implications for continental growth in the Central Asian Orogenic Belt: Lithos, v. 110, n. 1–4, p. 359–372, http://dx.doi.org/10.1016/j.lithos.2009.02.001
Wang, T., Tong, Y., Li, S., Zhang, J. J., Shi, X. J., Li, J. Y., Han, B. F., and Hong, D. W., 2010, Spatial and temporal variations of granitoids in the Altay orogen and their implications for tectonic setting and crustal growth: perspectives from Chinese Altay: Acta Petrologica et Mineralogica, v. 29, n. 6, p. 595–618.
Wang, W., Wei, C. J., Wang, T., Lou, Y. X., and Chu, H. G., 2009b, Confirmation of pelitic granulite in the Altai orogen and its geological significance: Chinese Science Bulletin, v. 54, n. 14, p. 2543–2548, http://dx.doi.org/10.1007/s11434-009-0041-6
Whalen, J. B., Currie, K. L., and Chappell, B. W., 1987, A-type granites: geochemical characteristics, discrimination and petrogenesis: Contributions to Mineralogy and Petrology, v. 95, n. 4, p. 407–419, http://dx.doi.org/10.1007/BF00402202
White, A. J. R., and Chappell, B. W., 1988, Some supracrustal (S-type) granites of the Lachlan Fold Belt: Transactions of the Royal Society of Edinburgh—Earth Sciences, v. 79, n. 2–3, p. 169–181, http://dx.doi.org/10.1017/S026359330001419X
Wickham, S. M., Alberts, A. D., Zanvilevich, A. N., Litvinovsky, B. A., Bindeman, I. N., and Schauble, E. A., 1996, A stable isotope study of anorogenic magmatism in East Central Asia: Journal of Petrology, v. 37, n. 5, p. 1063–1095, http://dx.doi.org/10.1093/petrology/37.5.1063
Windley, B. F., Kröner, A., Guo, J. H., Qu, G. S., Li, Y., and Zhang, C., 2002, Neoproterozoic to Palaeozoic geology of the Altai orogen, NW China: New zircon age data and tectonic evolution: The Journal of Geology, v. 110, n. 6, p. 719–737, http://dx.doi.org/10.1086/342866
Wu, F. Y., Jahn, B. M., Wilde, S., and Sun, D. Y., 2000, Phanerozoic crustal growth: U-Pb and Sr-Nd isotopic evidence from the granites in northeastern China: Tectonophysics, v. 328, n. 1–2, p. 89–113, http://dx.doi.org/10.1016/S0040-1951(00)00179-7
Wu, F. Y., Sun, D. Y., Jahn, B. M., and Wilde, S., 2004, A Jurassic garnet-bearing granitic pluton from NE China showing tetrad REE patterns: Journal of Asian Earth Sciences, v. 23, n. 5, p. 731–744, http://dx.doi.org/10.1016/S1367-9120(03)00149-4
Wu, F. Y., Yang, Y. H., Xie, L. W., Yang, J. H., and Xu, P., 2006, Hf isotopic compositions of the standard zircons and baddeleyites used in U-Pb geochronology: Chemical Geology, v. 234, n. 1–2, p. 105–126, http://dx.doi.org/10.1016/j.chemgeo.2006.05.003
Xiao, W. J., Windley, B. F., Badarch, G., Sun, S., Li, J., Qin, K., and Wang, Z., 2004, Palaeozoic accretionary and convergent tectonics of the southern Altaids: implications for the growth of Central Asia: Journal of the Geological Society, London, v. 161, n. 3, p. 339–342, http://dx.doi.org/10.1144/0016-764903-165
Xiao, W. J., Han, C. M., Yuan, C., Sun, M., Lin, S. F., Chen, H. L., Li, Z. L., Li, J. L., and Sun, S., 2008, Middle Cambrian to Permian subduction-related accretionary orogenesis of Northern Xinjiang, NW China: Implications for the tectonic evolution of central Asia: Journal of Asian Earth Sciences, v. 32, n. 2–4, p. 102–117, http://dx.doi.org/10.1016/j.jseaes.2007.10.008
Xiao, W. J., Windley, B. F., Yuan, C., Sun, M., Han, C. M., Lin, S. F., Chen, H. L., Yan, Q. R., Liu, D. Y., Qin, K. Z., Li, J. L., and Sun, S., 2009, Paleozoic multiple subduction-accretion processes of the southern Altaids: American Journal of Science, v. 309, n. 5, p. 221–270, http://dx.doi.org/10.2475/03.2009.02
Xiao, W. J., Huang, B. C., Han, C. M., Sun, S., and Li, J. L., 2010, A review of the western part of the Altaids: A key to understanding the architecture of accretionary orogens: Gondwana Research, v. 18, n. 2–3, p. 253–273, http://dx.doi.org/10.1016/j.gr.2010.01.007
Xiao, X. C., Tang, Y. Q., Feng, Y., Zhu, B., Li, J., and Zhou, M., 1992, Tectonics in northern Xinjiang and its neighbouring areas: Beijing, Geological Publishing, p. 104–121 (in Chinese with English abstract).
Xu, J. F., Castillo, P. R., Chen, F. R., Niu, H. C., Yu, X. Y., and Zhen, Z. P., 2003, Geochemistry of late Paleozoic mafic igneous rocks from the Kuerti area, Xinjiang, northwest China: implications for backarc mantle evolution: Chemical Geology, v. 193, n. 1–2, p. 137–154, http://dx.doi.org/10.1016/S0009-2541(02)00265-6
Yakubchuk, A., 2004, Architecture and mineral deposit settings of the Altaid orogenic collage: a revised model: Journal of Asian Earth Sciences, v. 23, n. 5, p. 761–779, http://dx.doi.org/10.1016/j.jseaes.2004.01.006
Yang, J. H., Wu, F. Y., Wilde, S. A., Xie, L. W., Yang, Y. H., and Liu, X. M., 2007, Tracing magma mixing in granite genesis: *in situ* U–Pb dating and Hf-isotope analysis of zircons: Contributions to Mineralogy and Petrology, v. 153, n. 2, p. 177–190, http://dx.doi.org/10.1007/s00410-006-0139-7
Yarmolyuk, V. V., Kovalenko, V. I., Sal'nikova, E. B., Budnikov, S. V., Kovach, V. P., Kotov, A. B., and Ponomarchuk, V. A., 2002, Tectono-Magmatic zoning, magma sources and geodynamics of the Early Mesozoic Mongolia-Trasbaikal province: Geotectonics, v. 36, n. 4, p. 293–311.
Yarmolyuk, V. V., Kovalenko, V. I., Kozlovskii, A. M., Vorontsov, A. A., and Savatenkov, V. M., 2005, Late Paleozoic–Early Mesozoic rift system of the Central Asia: composition and source of magmatism, development trends and geodynamics, *in* Kovalenko, V. I., editor, Tectonic Problems of Central Asia: Moscow, World of Science Publisher, Geosciences, p. 197–232.
Yarmolyuk, V. V., Kovalenko, V. I., Anisimova, I. V., Sal'nikova, E. B., Kovach, V. P., Kozakov, A. M., Kozlovsky, E. A., Kudryashova, E. A., Kotov, A. B., Plotkina, Y. V., Terent'eva, L. B., and Yakovleva, S. Z., 2008, Late Riphean alkali granites of the Zabhan microcontinent: evidence for the timing of Rodinia breakup and formation of microcontinents in the Central Asian Fold Belt: Doklady Earth Sciences, v. 420, n. 1, p. 583–588. http://dx.doi.org/10.1134/S1028334X08040132
Yu, X. Y., Mei, H. J., Yang, X. C., and Wang, J. D., 1993, Irtysh volcanic rocks and tectonic evolution, *in* Tu, G. Z., editor, Progress of solid-earth sciences in northern Xinjiang, China: Beijing, Science Press, p, 185–198 (in Chinese with English abstract).
Yuan, C., Sun, M., Xiao, W. J., Li, X. H., Chen, H. L., Lin, S. F., Xia, X. P., and Long, X. P., 2007, Accretionary

orogenesis of the Chinese Altai: Insights from Paleozoic granitoids: Chemical Geology, v. 242, n. 1–2, p. 22–39, http://dx.doi.org/10.1016/j.chemgeo.2007.02.013

Yuan, C., Sun, M., Xu, Y., Zhao, G. C., Xiao, W. J., Long, X. P., and Yin, Y., 2011, Oceanic lithospheric mantle beneath the continental crust of the Chinese Altai: Journal of the Geological Society, v. 168, n. 4, p. 995–1000, http://dx.doi.org/10.1144/0016-76492010-058

Yuan, H. L., Gao S., Liu, X. M., Li, H. M., Günther, D., and Wu, F. Y., 2004, Accurate U-Pb age and trace element determinations of zircon by laser ablation–inductively coupled plasma mass spectrometry: Geostandards and Geoanalytical Research, v. 28, n. 3, p. 353–370, http://dx.doi.org/10.1111/j.1751-908X.2004.tb00755.x

Zhang, Q. F., Hu, A. Q., Zhang, G. X., Fan, S. K., Pu, Z. P., and Li, Q., 1994, Evidence from isotopic age for presence of Mesozoic-Cenozoic magmatic activities in Altai region, Xinjiang: Geochimica, v. 23, n. 3, p. 269–280.

Zheng, Y. F., Zhang, S. B., Zhao, Z. F., Wu, Y. B., Li, X., Li, Z., and Wu, F. Y., 2007, Contrasting zircon Hf and O isotopes in the two episodes of Neoproterozoic granitoids in South China: implications for growth and reworking of continental crust: Lithos, v. 96, n. 1–2, p. 127–150, http://dx.doi.org/10.1016/j.lithos.2006.10.003

Zhu, Y. F., Zeng, Y. S., and Gu, L. B., 2006, Geochemistry of the rare metal-bearing pegmatite No. 3 vein and related granites in the Keketuohai region, Altay Mountains, northwest China: Journal of Asian Earth Sciences, v. 27, n. 1, p. 61–77, http://dx.doi.org/10.1016/j.jseaes.2005.01.007

Zou, T. R., Chao, H. Z., and Wu, B. Q., 1988, Orogenic and anorogenic granitoids of Altay Mountains of Xinjiang and their discrimination criteria: Acta Geological Sinica, v. 2, n. 1, p. 45–64, http://dx.doi.org/10.1111/j.1755-6724.1989.mp2001005